

1 **Title:**

2 Pupil size predicts the onset of exploration and changes in prefrontal dynamics

3

4 **Authors:**

5 Akram Shourkeshti^{1†}, Mojtaba Abbaszadeh^{1†}, Gabriel Marrocco¹, Katarzyna Jurewicz^{1,2}, Tirin
6 Moore^{3,4}, R. Becket Ebitz^{*1}

7

8

9 **Affiliations:**

10 ¹Département de Neurosciences, Université de Montréal, Montréal, QC, Canada

11 ²Department of Physiology, McGill University, Montréal, QC, Canada

12 ³Department of Neurobiology, Stanford University School of Medicine, Stanford, CA, USA

13 ⁴Howard Hughes Medical Institute, Chevy Chase, MD, USA

14

15 [†] These authors contributed equally to this work.

16 *Corresponding author and lead contact:

17 R. Becket Ebitz

18 Department of Neurosciences

19 Université de Montréal

20 Montréal, QC CANADA H3T 1J4

21 Email: becket@ebitzlab.com

22

23

24 **Abstract**

25 In uncertain environments, intelligent decision-makers exploit actions that have been rewarding
26 in the past, but also explore actions that could be even better. Several neuromodulatory
27 systems are implicated in exploration, based, in part, on work linking exploration to pupil size—a
28 peripheral correlate of neuromodulatory tone and index of arousal. However, pupil size could
29 instead track variables that make exploration more likely, like volatility or reward, without directly
30 predicting either exploration or its neural bases. Here, we simultaneously measured pupil size,
31 exploration, and neural population activity in the prefrontal cortex while two rhesus macaques
32 explored and exploited in a dynamic environment. We found that pupil size under constant
33 luminance specifically predicted the onset of exploration, the first exploratory trial in a sequence,
34 beyond what could be explained by reward history. Pupil size also predicted disorganized
35 patterns of prefrontal neural activity at both the single neuron and population levels, even within
36 periods of exploitation. Ultimately, our results support a model in which pupil-linked mechanisms
37 promote the onset of exploration via driving the prefrontal cortex through a critical tipping point
38 where prefrontal control dynamics become disorganized and exploratory decisions are possible.

39 **Significance Statement**

40 Humans and other animals learn about the world through exploration: through making decisions
41 that offer the opportunity to learn and discover, even when these decisions are not the best
42 option in the moment. Neuroscience research has historically focused on understanding good
43 choices, delivering many key insights into the neural mechanisms involved in these calculations.
44 However, much less is known about how the brain generates exploratory decisions. This study
45 identifies certain “early warning signs” of exploratory decisions in the brain and body, including
46 certain signals in size of the pupil and the speed of neural activity in the prefrontal cortex. These
47 early warning signs suggest that exploration may be the result of a critical tipping point in
48 prefrontal brain states.

49 **Introduction**

50 Many decisions maximize immediate rewards. However, in uncertain or changing environments,
51 it is important to sacrifice some immediate rewards in order to learn about the value of
52 alternative options and discover new, more valuable strategies for interacting with the world. In

53 short, in complex environments, intelligent decision-makers exploit rewarding strategies, but
54 also explore alternative strategies that could be even better.

55 Because exploitation maximizes immediate reward, it can rely on the same value-based
56 decision-making processes that have been the subject of neurobiological studies for decades
57 (Ding and Hikosaka, 2006; Jurewicz et al., 2022; Platt and Glimcher, 1999; Roesch and Olson,
58 2007; Schultz et al., 2008). However, we are only just beginning to understand the neural bases
59 of exploration (Costa and Averbeck, 2020; Daw et al., 2006; Pearson et al., 2009; Wilson et al.,
60 2021, 2014). One clue is that many organisms seem to explore via random sampling
61 (Gershman, 2019; Wilson et al., 2021, 2014). Randomness is a critical component of
62 exploratory discovery in bird song and motor learning (Fiete et al., 2007; Wu et al., 2014), it can
63 perform about as well as more sophisticated strategies in many environments (Dayan and Daw,
64 2008), and humans and other primates tend to explore randomly even when more sophisticated
65 strategies are available (Ebitz et al., 2018; Wilson et al., 2014). There is some neurobiological
66 evidence linking random exploration to disorganized activity patterns in the prefrontal cortex
67 (Ebitz et al., 2019, 2018; Muller et al., 2019; Wilson et al., 2021), but we still do not understand
68 the proximate causes of random exploration and its neural correlates in the prefrontal cortex.

69 One promising hypothesis is that exploration could be under the control of some process(es)
70 linked to pupil size. Pupil size under constant luminance is a peripheral index of autonomic
71 arousal (Bradley et al., 2008; Ebitz and Moore, 2019; Loewenfeld, 1999) that also predicts
72 widespread changes in neural population activity (McGinley et al., 2015; Reimer et al., 2014)—
73 including in regions implicated in decision-making noise (Ebitz and Platt, 2015; Tervo et al.,
74 2014). Among other neuromodulators (Gilzenrat et al., 2010; Koss, 1986; Reimer et al., 2016),
75 pupil size is correlated with central norepinephrine (Costa and Rudebeck, 2016; Joshi et al.,
76 2016): a catecholamine that flattens neuronal tuning functions (Martins and Froemke, 2015) and
77 predicts “resets” in cortical networks (Aston-Jones and Cohen, 2005; Bouret and Sara, 2005).
78 Behaviorally, pupil size predicts decision-making noise (Aston-Jones and Cohen, 2005; Ebitz et
79 al., 2014; Eldar et al., 2013; Gilzenrat et al., 2010; O'Reilly et al., 2013; Wilson et al., 2021),
80 especially errors of reward-maximization (Jepma and Nieuwenhuis, 2011a) and task
81 performance (Ebitz et al., 2014; Ebitz and Platt, 2015). Some of these “errors” may be caused
82 by exploratory processes (Ebitz et al., 2019; Jepma and Nieuwenhuis, 2011a; Pisupati et al.,
83 2021).

84 There is a plausible alternative interpretation of this data: perhaps pupil size only tracks the
85 variables that make exploration more likely. Pupil size under constant luminance increases with
86 the volatility of reward environments, the surprise of reward outcomes, novelty, uncertainty, and
87 context changes (Clewett et al., 2020; Filipowicz et al., 2020; Graves et al., 2021; Preuschoff et
88 al., 2011; Slooten et al., 2018; Yokoi and Weiler, 2022): all variables that make exploration more
89 likely. However, it is often unclear whether the pupil is tracking these variables or instead
90 directly predicting behavioral changes like increased learning, decision-noise or exploration
91 (Nassar et al., 2012; O'Reilly et al., 2013; Urai et al., 2017). Fortunately, recent results suggest
92 that at least some exploration appears to occur tonically, regardless of these variables (Ebitz et
93 al., 2019; Pisupati et al., 2021; Wilson et al., 2021). Further, in parallel, new computational
94 approaches allows us to determine when exploration is occurring independently of the reward-
95 based computations thought to drive it (Chen et al., 2021; Ebitz et al., 2020, 2019, 2018). This
96 means that it is now possible to determine whether pupil size predicts exploration itself or
97 instead simply tracks the variables that make exploration more likely.

98 Here, we measured pupil size and recorded from populations of prefrontal neurons while two
99 rhesus macaques performed a task that encouraged exploration and exploitation. We found that
100 pupil size under constant luminance was larger during explore choices than exploit choices.
101 However, the temporal relationship between pupil size and exploration was both precise and
102 complex: spontaneous oscillations in pupil size entrained the onset of exploration. Together,
103 these results support the hypothesis that pupil-linked processes drive the prefrontal cortex
104 through a critical tipping point that permits exploratory decisions.

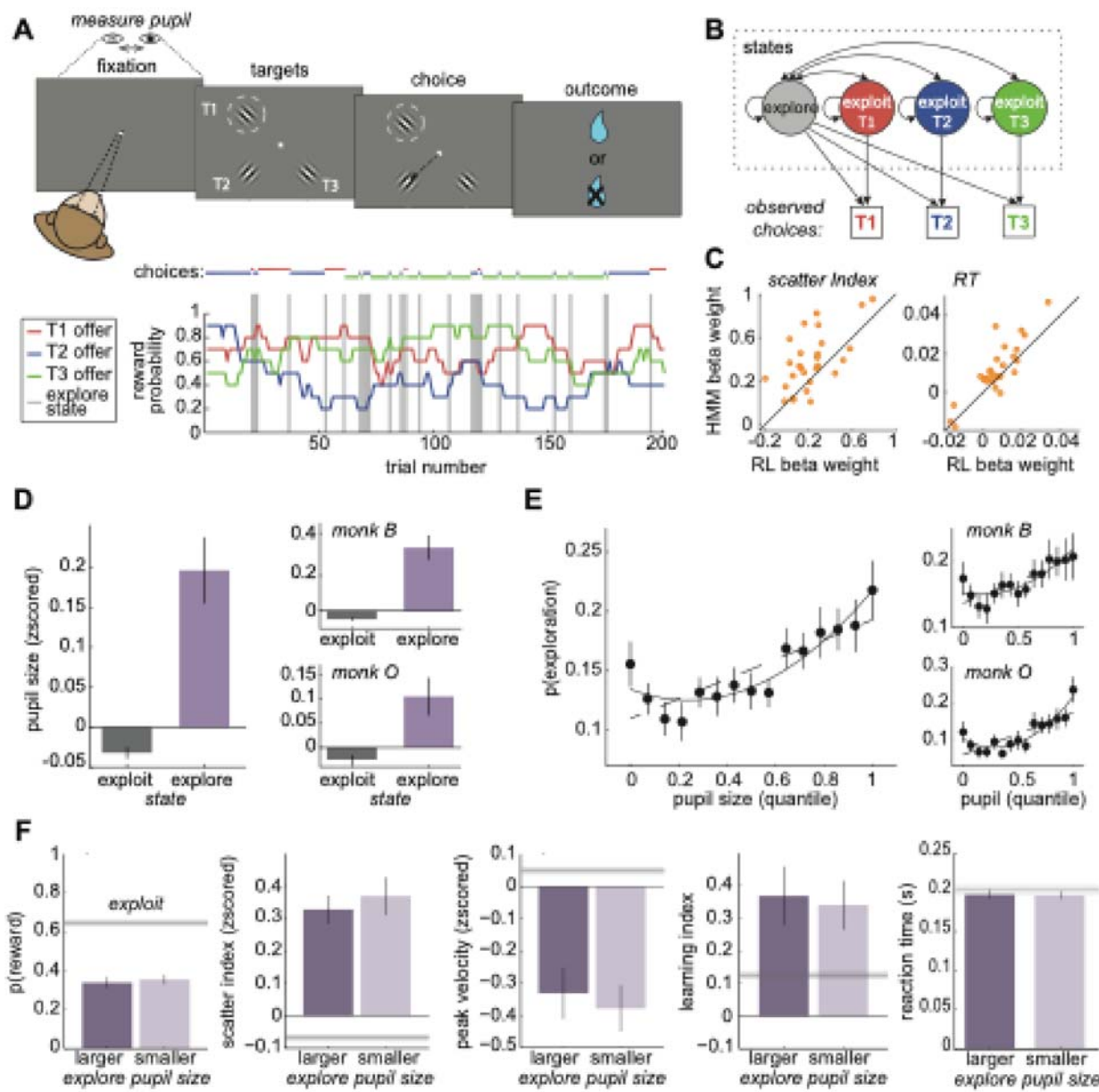
105 **Results**

106 Two male rhesus macaques performed a total of 28 sessions of a classic explore/exploit task: a
107 restless three-armed bandit (subject B: 10 sessions, subject O: 18 sessions; a total of 21,793
108 trials). Some analyses of this dataset have been reported previously (Ebitz et al., 2018), but the
109 pupil data has not been analyzed previously and all analyses presented here are new. In this
110 task, the reward probability (value) of three targets walks randomly and independently over time
111 (**Figure 1A**). This means that the subjects have to take advantage of valuable options when
112 they are available (exploit), but also occasionally sample alternative options to determine if they
113 have become more valuable (explore).

114 Rather than instructing subjects to explore and exploit, this task takes advantage of the
115 subjects' natural tendency to alternate between exploration and exploitation in a changing
116 environment. We have previously shown that both monkeys and mice exhibit 2 behavioral
117 modes in this task: one exploitative mode in which they repeatedly choose the same option—
118 learning little but maximizing reward—and one exploratory mode in which they alternate rapidly
119 between the options—choosing randomly with respect to rewards and learning rapidly (Chen et
120 al., 2021; Ebitz et al., 2018). We infer which of these modes is driving behavior with a hidden
121 Markov model (HMM; **Figure 1B**; see **Methods**). This approach models the exploratory and
122 exploitative modes as latent goal states and the maximum *a posteriori* goal is taken as the state
123 label for each choice. We have previously shown that this method identifies explore/exploit state
124 labels that match normative definitions (Chen et al., 2021; Ebitz et al., 2018) and explain
125 variance in prefrontal neural activity that cannot be explained by reward value, reward history,
126 and switch/stay decisions (Ebitz et al., 2018). This task design naturally elicits exploration and
127 exploitation, allowing us to investigate variability in pupil size and neural activity under both
128 conditions.

129 Some previous studies used a different method to identify exploratory choices (Daw et al., 2006;
130 Jepma and Nieuwenhuis, 2011a; Pearson et al., 2009). These studies fit a reinforcement
131 learning (RL) model to the behavior and identified the choices that are not consistent with the
132 model's subjective values as exploratory. However, this previous RL-based approach (1)
133 equates exploration with errors of reward maximization, not a goal that is orthogonal to reward
134 maximization, and (2) its accuracy depends on precise knowledge of the computations involved
135 in the choice, which are highly variable, both across individuals and over time (Chen et al.,
136 2021, 2021; Kaske et al., 2022). The HMM approach, conversely, makes no assumptions about
137 the computations involved in the choice and identifies choices that are orthogonal to reward
138 value, not anti-correlated with it (Chen et al., 2021; Ebitz et al., 2018). Here, we found that state
139 labels from the HMM method explained more variance in behavior and neural activity than
140 choice labels from the previous, RL method (**Figure 1C**; response time: both subjects, paired t-
141 test: $p < 0.005$, $t(27) = 3.41$, the mean difference of beta weights = 0.004, 95% CI = 0.002 to
142 0.007; scatter index [(Ebitz et al., 2018)]: both subjects, paired t-test: $p < 0.001$, $t(27) = 3.84$, the
143 mean difference of beta weights = 0.15, 95% CI = 0.07 to 0.24: see **Methods**). In short, we find
144 that the HMM approach is a more robust and accurate method, with better face validity, than the
145 RL-based method for identifying explore choices. Therefore, here, we used this more precise

146 approach to determine whether physiological signals, like pupil size, reliably track exploratory
 147 behavior.



149 **Figure 1. Task design and pupil.** A) Top: Subjects made saccadic choices between three
 150 identical options (T1, T2, and T3). One of the options (e.g., T1 in this example trial) was located
 151 in the receptive field of a neuron in the frontal eye field (FEF; dotted circle). Bottom: Reward
 152 probabilities for the 3 options (lines), with choices overlaid (dots) for 200 example trials. Gray
 153 bars = explore-labels. B) The HMM models exploration and exploitation as latent goal states
 154 underlying choice sequences. C) Comparison of regression coefficients for HMM-inferred and
 155 RL-inferred explore choices, predicting either the disorganization of neural population responses
 156 (“scatter index”; see Methods; Ebitz et al., 2018) or response time. Beta weights were obtained
 157 from session-level generalized linear models (GLMs) with explore state as the predictor (0 =

158 exploit, 1 = explore). Separate GLMs were fitted using explore labels from the HMM and from
159 an RL-based model. D) Average pupil size on explore and exploit choices. Right: Same for
160 individual subjects. E) The probability of explore choices as a function of pupil size quantile.
161 Dotted line: linear GLM fit. Solid line: quadratic fit. Right: Same for individual subjects. F)
162 Several behavior measures compared across median-split large- and small-pupil-size explore
163 choices. Left to right: reward probability, a one-trial-back learning index (see Methods), saccadic
164 peak velocity of saccades, the scatter index, and reaction time. No significant differences
165 between pupil bins. The grey line is the mean \pm SEM for exploit choices. Error bars depict \pm
166 SEM throughout.

167 Pupil size is larger during exploratory states

168 Having established that the HMM reliably distinguishes explore and exploit states, we next
169 asked whether pupil size changes across these behavioral states. Previous work using RL-
170 based labels reported that pupil size under constant luminance is larger during exploration than
171 exploitation (Jepma and Nieuwenhuis, 2011b). We therefore tested whether this pattern holds
172 using HMM-based labels in our dataset. Indeed, we found that pupil size at fixation (see
173 **Methods**) was larger on explore-labeled trials than exploit-labeled trials in both subjects (**Figure 1D**;
174 both subjects, paired t-test: $p < 0.0001$, $t(27) = 4.95$, mean offset = 0.23, 95% CI = 0.13 to
175 0.32; subject B: $p < 0.001$, $t(9) = 5.50$, mean offset = 0.4, 95% CI = 0.24 to 0.57; subject O: $p <$
176 0.02, $t(17) = 2.85$, mean offset = 0.13, 95% CI = 0.03 to 0.23). Thus, pupil size was larger
177 during exploratory choices identified with the HMM method.

178 However, the probability of exploration did not increase linearly as a function of pupil size
179 (**Figure 1E**). A linear, first-order GLM confirmed that larger pupil size generally predicted more
180 explore choices (both subjects: $\beta = 0.084$, $p < 0.0001$, AIC = -1053.70, $n = 28$ sessions). This
181 relationship held when analyzed separately in each subject (subject B: $\beta = 0.063$, $p = 0.002$, AIC
182 = -368.01, $n = 10$ sessions; subject O: $\beta = 0.110$, $p < 0.0001$, AIC = -249.46, $n = 18$ sessions).
183 Yet the relationship was clearly nonlinear. A quadratic model provided a significantly better fit
184 than the linear model for the combined dataset (2nd order GLM: $\beta_1 = -0.081$, $p = 0.101$; $\beta_2 =$
185 0.166, $p = 0.0006$; AIC = -1063.62, AIC weight for the quadratic model = 0.993), consistent with
186 a U-shaped relationship. This U-shape was especially prominent in subject O ($\beta_1 = -0.13$, $p =$
187 0.090; $\beta_2 = 0.240$, $p = 0.001$; AIC = -258.01), although the quadratic model was not an
188 improvement over the linear model in subject B ($\beta_1 = -0.027$, $p = 0.709$; $\beta_2 = -0.091$, $p = 0.205$;
189 AIC = -367.63).

190 In order to determine whether this pattern was also apparent in the raw data (i.e. not the HMM-
191 model labels), we next examined how pupil size predicted switching behavior—i.e., choosing a

192 different option than in the previous trial. We again observed a U-shaped relationship between
193 pupil size and the probability of making a switch choice in both subjects (1st-order GLM: $\beta =$
194 0.084 , $p < 0.0001$, $n = 28$ sessions; subject B: $\beta = 0.0800$, $p < 0.0001$; subject O: $\beta = 0.0807$, p
195 < 0.0001). A 2nd-order quadratic model provided a superior fit in both animals (both subjects: β_1
196 $= -0.099$, $p = 0.023$; $\beta_2 = 0.184$, $p < 0.0001$; subject B: $\beta_1 = -0.069$, $p = 0.284$, $\beta_2 = 0.149$, $p =$
197 0.010 ; subject O: $\beta_1 = -0.093$, $p = 0.103$, $\beta_2 = 0.174$, $p = 0.001$). Model comparison strongly
198 favored the quadratic model (linear AIC = -1195.05 ; quadratic AIC = -1211.95 ; AIC weight for
199 quadratic model = 0.9998). Thus, although pupil size tended to be larger during exploration than
200 exploitation, its relationship with both exploration and switching was clearly U-shaped.

201 One possible explanation for the U-shaped pattern is that some “explore” choices—particularly
202 those with small pupil size—reflect disengagement at low levels of arousal, rather than true
203 exploration. However, if this were the case, then the valid, large-pupil explore choices would
204 systematically differ from the false, small-pupil “explore” choices. They did not. To evaluate this
205 possibility, we compared small- and large-pupil explore trials across several behavioral
206 dimensions known to be sensitive to lapses in task engagement. These included reward rate,
207 saccade velocity, the neural scatter index, a trial-wise learning index, reaction time—each
208 previously associated with arousal, motivation, or task-related updating (Chen et al., 2021; Ebitz
209 et al., 2018; Laurie et al., 2025). Small- and large-pupil explore choices (median split) were
210 indistinguishable along several of the key dimensions that differentiate explore choices from
211 exploit choices (**Figure 1F**). For example, both were equally likely to be rewarded (mean
212 difference = 0.03 ± 0.24 STD) between large- and small pupil-explore choices ($p > 0.4$, $t(1,27) =$
213 0.75 , paired t-test; AUC for discriminating explore and exploit = 0.65 ± 0.05 STD across
214 sessions). Both had similar peak saccadic velocities (mean difference = -0.05 ± 0.23 STD, $p >$
215 0.2 , $t(27) = -1.08$; explore/exploit AUC = 0.61 ± 0.10 STD) and both had more variability in
216 neural population choice information (“scatter index”, mean difference = 0.03 ± 0.33 STD, $p >$
217 0.6 , $t(27) = 0.45$; explore/exploit AUC = 0.60 ± 0.07 STD). Both had similar levels of reward
218 learning (see **Methods**; the mean difference = -0.03 ± 0.57 STD, $p > 0.7$, $t(27) = 0.27$): in both
219 cases, learning was substantially enhanced relative to the exploit choices (small-pupil, the mean
220 difference from exploit = 0.24 ± 0.48 STD, $p < 0.02$, $t(27) = 2.69$; large-pupil, the mean
221 difference from exploit = 0.21 ± 0.39 STD, $p < 0.01$, $t(27) = 2.91$). Reaction times were also
222 similar across small- and large-pupil explore choices (mean difference = 0.01 ± 0.02 STD, $p >$
223 0.6 , $t(27) = 1.84$; explore/exploit AUC = 0.58 ± 0.06 STD). These results are incompatible with
224 the idea that either type of explore choice reflects disengagement in the task or that small- and

225 large-pupil explore choices have different causes. Instead, we will see that the U-shape was
226 due to the complex temporal relationship between pupil size and exploration.

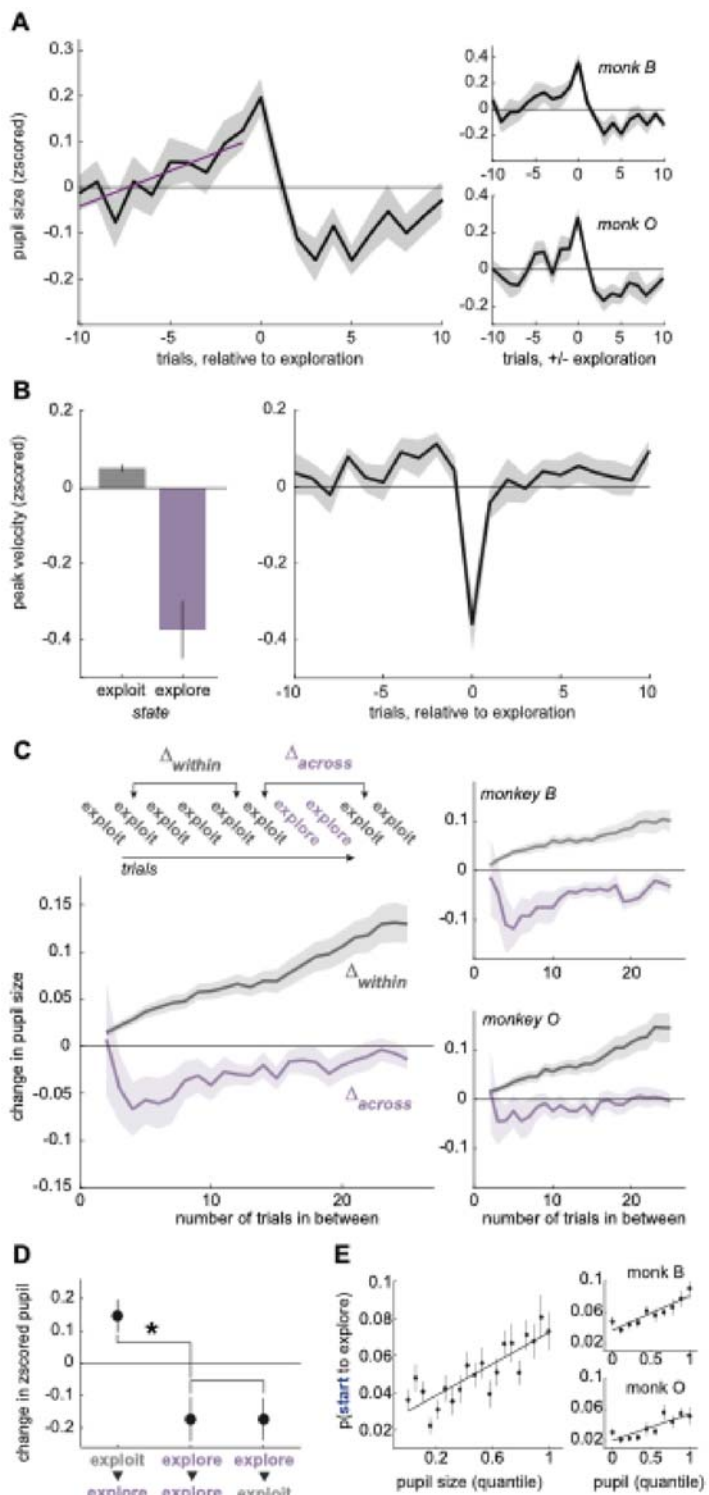
227 **Pupil size, but not other measures ramp up before exploration**

228 Pupil size ramped up across trials before exploration began in both subjects. After exploration, it
229 shrank to below-baseline levels when exploitation resumed (**Figure 2A**). Here, "baseline" refers
230 to a z-scored value of 0, computed by subtracting the session mean and dividing by the session
231 standard deviation of pupil size (see **Methods**). This ramping meant that pupil size was larger
232 not just during exploration, but also during the exploit choices immediately before exploration
233 (both subjects, GLM slope = 0.01, $p < 0.005$, $n = 28$; subject B: beta = 0.02, $p < 0.02$, $n = 10$;
234 subject O: beta = 0.01, $p < 0.05$, $n = 18$; average pupil size compared to the exploit choices,
235 post-hoc paired t-tests, 1 trial before exploration mean = 0.12, $p < 0.005$, $t(27) = 3.42$; 2 trials
236 mean = 0.09, $p < 0.03$, $t(27) = 2.41$; 3 trials mean = 0.03, $p > 0.1$, $t(27) = 1.42$; 4 trials mean =
237 0.05, $p < 0.05$, $t(27) = 2.07$). By the first exploit choice after exploration, pupil size had already
238 begun shrinking to below-baseline levels (post-hoc paired t-tests, 1 trial after exploration mean
239 = 0.03, $p = 0.09$, $t(27) = 1.73$; 2 trials after mean = -0.11, $p < 0.02$, $t(27) = -2.67$; 3 trials after
240 mean = -0.16, $p < 0.02$, $t(27) = -2.72$; 4 trials after mean = -0.08, $p > 0.2$, $t(27) = -1.27$; 5 trials
241 after mean = -0.16, $p < 0.001$, $t(27) = -3.94$; p-values are significant with a Holm-Bonferroni
242 correction). The shrinking to below-baseline levels could suggest a refractory mechanism that
243 would prevent exploration from re-occurring immediately after it happened.

244 To rule out potential confounds, we tested whether the pupil ramping and shrinking effects could
245 be explained by misaligned labels or unrelated behavioral dynamics. We saw no evidence of
246 ramping in peak saccadic velocity, another behavioral measure that differentiated explore trials
247 and exploit trials (**Figure 2B**; no significant decrease from baseline 1 trial before, paired t-test: p
248 > 0.7 , $t(27) = 0.42$; a GLM was nonsignificant with the trend pointing in the opposite direction: 10
249 trials preceding exploration, beta = 0.008, $p > 0.1$) and no significant change from baseline
250 afterward (not greater than the baseline during the 5 trials after exploration, when pupil shrinking
251 was maximal, mean = -0.47 ± 0.15 STD, $p > 0.9$, one-sided $t(27) = -1.67$). We previously
252 reported similar results for decoded choice probability and the scatter index (see **Methods**) in
253 neurons of the frontal eye field (FEF), a prefrontal cortex region involved in directing gaze and
254 attention (Ebitz et al., 2018). Thus, while pupil size ramped before exploration began and shrank
255 afterward, the same was not true of other behavioral and neural variables, suggesting that these
256 dynamics were not some artifact of misalignment.

257 **Pupil size generally ramps across trials, but resets with exploration**

258 To better understand whether pupil ramping was a general feature of arousal dynamics or
259 specific to exploration, we examined how pupil size evolved across trials with and without
260 exploratory transitions (see **Methods**). When the subjects did not explore the pupil size
261 increased steadily across trials (**Figure 2C**;
262 both subjects, GLM: $\beta = 0.004$, $p < 0.0001$; subject B: $\beta = 0.003$, $p < 0.0001$;
263 subject O: $\beta = 0.005$, $p < 0.0001$, $n = 25$
264 lags over 28 sessions). This implies that the
265 ramping in pupil size before explore choices
266 may be a general dynamic of how pupil size
267 evolves in the absence of exploration.
268 However, a different pattern emerged when
269 we looked at how the pupil changed
270 between exploit trials that were separated
271 by exploration. When two exploit trials were
272 separated by at least one explore choice,
273 pupil size was smaller on the second exploit
274 trial (both subjects, GLM: $\beta = -0.09$, $p < 0.0001$; subject B: $\beta = -0.14$, $p < 0.0001$;
275 subject O: $\beta = -0.07$, $p < 0.0001$).
276 Critically, passing through exploration only
277 produced a baseline decrease in pupil size
278 but did not alter the rate at which pupil size
279 grew over trials (no significant interaction
280 between slope and condition in both
281 subjects, GLM: $\beta < -0.0001$, $p > 0.9$;
282 subject B: $\beta = 0.003$, $p < 0.05$; subject O:
283 $\beta = -0.002$, $p > 0.1$; also nonsignificant
284 on trials 5-25: both subjects: $\beta < 0.0005$,
285 $p > 0.5$). Therefore, pupil size tended to
286 ramp across trials but exploratory choices



289 temporarily decreased pupil size without disrupting this ramping in the long term.

290 **Figure 2. Pupil size ramps up before exploration and shrinks down after.** A) Average pupil
291 size for 10 trials before and 10 trials after explore choices. Purple line: GLM fit. Right: Same for
292 each subject separately. B) Same as **Figures 1D** and **2A** but for peak velocity rather than pupil
293 size. C) Change in pupil size between exploit trials that are either in a single bout of exploitation
294 (gray) or separated by explore trials (purple). Right: Same for each subject separately. D)
295 Change in pupil size over certain pairs of trials: starting (exploit to explore), during (explore to
296 explore), and leaving (explore to exploit) exploration. * $p < 0.001$ E) The probability of starting to
297 explore as a function of pupil size quantile. Solid line: Linear GLM fit. Error bars and shaded
298 regions depict mean \pm SEM. Insets: Same analysis shown separately for each monkey.

299 **Pupil size specifically predicts the onset—not the maintenance—of exploration**

300 Pupil size tends to be smaller after exploration, but this shrinkage could either be driven by the
301 end of exploration (i.e. the start of exploitation) or it could begin shortly after the beginning of
302 exploration itself. If the pupil starts to shrink only after exploration ends, it would support models
303 that suggest that pupil size decreases with commitment to a new option or belief state (O'Reilly
304 et al., 2013). Conversely, if the pupil shrinks immediately after exploration begins, it might
305 suggest that pupil-linked mechanisms are important for initiating exploration, but not sustaining
306 it. Our results were consistent with the latter hypothesis: the pupil immediately began shrinking
307 as soon as exploration began, not when it ended (**Figure 2D**; mean change in pupil size
308 between neighboring explore choices = -0.17, t-test, $t(27) = -2.69$, $p < 0.02$; 95% CI = -0.30 to -
309 0.04). This was essentially identical to the magnitude with which the pupil shrank on exploit
310 trials that followed explore trials (mean change = -0.17, t-test, $t(27) = -2.56$, $p < 0.02$; 95% CI = -
311 0.31 to -0.03). Validating the ramping we observed with other methods, we also found that pupil
312 size tended to grow on explore trials that followed exploit trials here (mean change = 0.14, t-
313 test, $t(27) = 2.96$, $p < 0.01$; 95% CI = 0.04 to 0.24). Together, these results suggest that pupil
314 size and pupil-linked mechanisms specifically predict the “onset” of exploration—the first
315 exploratory trial in a sequence—and may not be important for sustaining exploration after the
316 first explore choice.

317
318 The tendency of the pupil to shrink after the onset of exploration could explain the previously
319 noted U-shaped relationship between pupil size and exploration. In this view, the small-pupil-
320 size explore choices would be the later explore choices in a sequence and the larger pupil size
321 explore choices would tend to be the first explore choice(s). Indeed, pupil size had a primarily
322 linear relationship with the onset of exploration in both subjects (**Figure 2E**; 1st order GLM: $\beta =$
323 0.042, $p < 0.0001$, AIC = -1973.57). Adding a quadratic term did not substantially improve the

324 model fit ($\beta_2 = 0.038$, $p = 0.073$; quadratic model AIC = -1974.81 ; $\Delta\text{AIC} = -1.24$; AIC weight of
325 quadratic model = 0.65; see **Methods**). This linear relationship was also observed in both
326 monkeys individually (see **Figure 2E**, right panels). For subject B, a first order GLM confirmed a
327 significant positive association ($\beta = 0.044$, $p < 0.0001$, AIC = -699.13), and adding a quadratic
328 term did not improve the model fit ($\beta_2 = 0.049$, $p = 0.0878$; $\Delta\text{AIC} = -0.96$). Similarly, for subject
329 O, pupil size showed a significant linear relationship with exploration onset ($\beta = 0.034$, $p <$
330 0.0001 , AIC = -460.29), and the quadratic model again provided no additional explanatory
331 power ($\beta_2 = 0.022$, $p = 0.402$; $\Delta\text{AIC} = +1.30$). These results confirm that the linear relationship
332 between pupil size and the onset of exploration was robust across both subjects and not driven
333 by outliers or subject-specific variability. Conversely, there was no special relationship between
334 pupil size and probability of starting to exploit (1st order GLM: beta = 0.05, $p > 0.05$). Thus, pupil
335 size specifically predicted the onset of exploration, rather than explore choices or state switches
336 more generally.

337 If the U-shaped relationship between pupil size and exploration (**Figure 1E**) were driven
338 primarily by later explore trials, it should remain evident after excluding onset trials from the
339 analysis. Moreover, removing onsets should substantially reduce the slope of the linear effect.
340 To test this, we repeated the analysis using only later explore trials. As expected, the linear
341 slope decreased in both subjects (**Figure S1**): for subject B, β_1 dropped from 0.063 (all explore
342 trials) to 0.018 (excluding onsets), and for subject O, from 0.110 to 0.075. In contrast, the
343 quadratic terms remained relatively stable: for subject B, β_2 was 0.091 for all explore trials and
344 0.041 with onsets excluded; for subject O, β_2 was 0.240 and 0.215, respectively. Importantly,
345 the U-shaped relationship persisted when data were combined across both subjects (**Figure**
346 **S1**), with the quadratic model significantly outperforming the linear model
347 ($\beta_2=0.121, p=0.012 \backslash \beta_2 = 0.121, p = 0.012 \backslash \beta_2=0.121, p=0.012$; AIC = -878.78 vs. -874.55 ;
348 AIC weight for the quadratic model = 0.893). These findings confirm that the nonlinearity
349 observed in the original analysis (**Figure 1E**) was driven by the decrease in pupil size in later
350 exploratory trials, whereas the onset of exploration had a largely linear relationship with pupil
351 size.

352 **Exploration is gated by pupil-linked arousal, not just reward history**

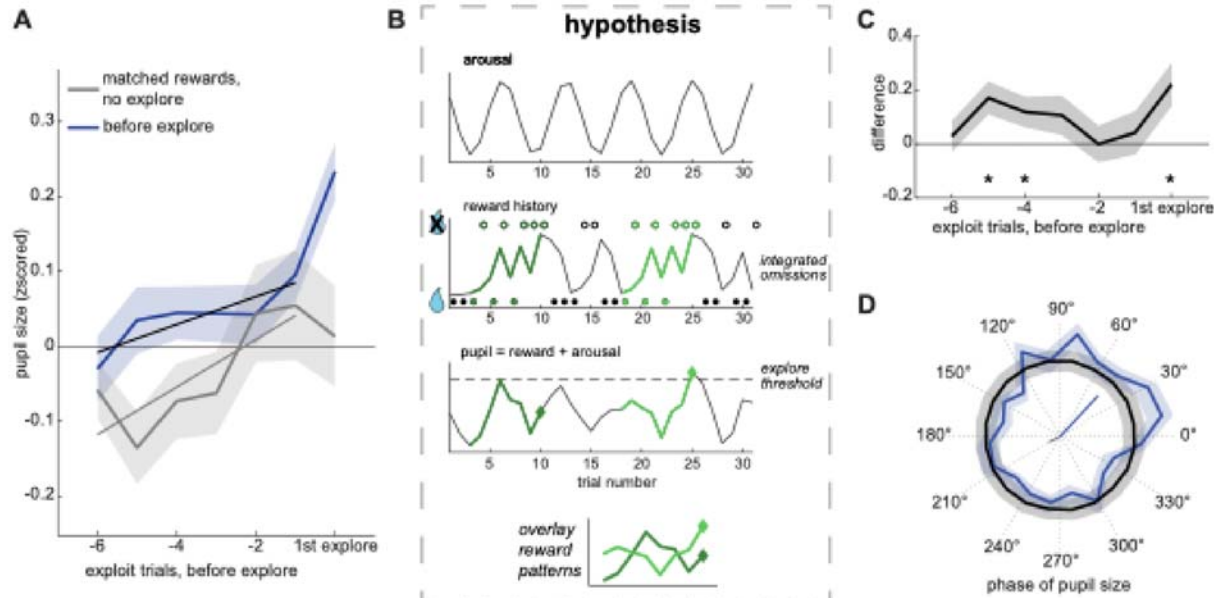
353 Although pupil size predicted the onset of exploration, it remained possible that this relationship
354 was driven by a shared sensitivity to recent reward outcomes, since both exploration (Daw et
355 al., 2006; Ebitz et al., 2018; Wilson et al., 2014) and pupil dilation (Bijleveld et al., 2009; Jepma

356 and Nieuwenhuis, 2011b) tend to increase following reward omission. To determine if there was
357 a direct effect of pupil-related processes on exploration, we compared pupil size across exploit
358 trials before exploration with pupil size from matched trial sequences where exploration did not
359 happen (see **Methods**). There was a significant increase in pupil size during the trials before
360 exploration compared to “matched rewards” control trials (**Figure 3B**; GLM, beta = 0.025, p <
361 0.01, n = 28), suggesting that pupil size predicted the onset of exploration beyond what could be
362 explained by reward. Again, pupil size ramped up over time (GLM, beta = 0.119, p < 0.02, n =
363 28), but this ramping did not differ between the traces (GLM, beta = 0.007, p > 0.5, n = 28). This
364 implies that either reward history or time (i.e., the number of trials) may explain the pupil
365 ramping before exploration, although there is still an offset in pupil size that predicts the onset of
366 exploration above and beyond the effect of reward history.

367 Visual inspection of **Figure 3A** suggested that there may be a phase difference in pupil size
368 between trials where exploration began and matched reward trials where exploration did not
369 begin. This led us to develop a novel hypothesis (**Figure 3B**): that rewards may interact with
370 ongoing oscillations in pupil size. Due to delays in communication between the baroreceptor
371 reflect and changes in heart rate, the sympathetic nervous system (Borjon et al., 2016;
372 Japundzic et al., 1990; Julien, 2020, 2006; Kamiya et al., 2005; Liao et al., 2018) has a natural
373 oscillation known as the Mayer wave, with a period of approximately 0.05–0.1 Hz (Borjon et al.,
374 2016b; Julien, 2006). Critically, transitions in other behavioral states can be entrained by this
375 oscillation, with eliciting stimuli causing transitions only at certain phases of arousal. This view
376 predicts that the previous trials most predictive of the onset of exploration may actually be
377 several trials prior to onset itself—during the periods in which the signals are most out of phase.
378 Indeed, the trials in which pupil size best predicted the onset of exploration were not those
379 immediately preceding it (e.g., trial t-1 or t-2), but rather trials t-4 and t-5 (**Figure 3C**; trial t-4,
380 mean difference = 0.117, p < 0.05, t(27) = 2.09; trial t-5 = 0.170, p < 0.01, t(27) = 2.84).

381 The view that omitted rewards only evoke exploration when they coincide with particular phases
382 of sympathetic arousal also implies that the onset of exploration should be phase-locked to
383 the Mayer wave frequency (see **Methods**). The median trial duration was ~3 seconds (range =
384 [2.2, 3.2]), so a ~5-trial cycle would correspond to a 0.06–0.09 Hz oscillation, which aligns with
385 the frequency range of the Mayer wave. We found that pupil phase at the onset of exploration
386 was concentrated at the rising phase (**Figure 3D**; mean phase = 47.18°, Hodges-Ajne test, p <
387 0.01; vector length = 0.075; null = 0.026, 95% CI = 0.004 to 0.057, p < 0.0001). In contrast, pupil
388 phases during reward-matched trials pointed in the opposite direction (mean phase = 207.58°;

389 significantly different from onsets, $p < 0.02$, Watson's $U^2 = 0.25$, $n = 2170$ phases including
390 1135 onsets). Together, these results support the hypothesis (**Figure 3B**) that slow, rhythmic
391 fluctuations in arousal interact with reward history to determine the timing of exploration onset.



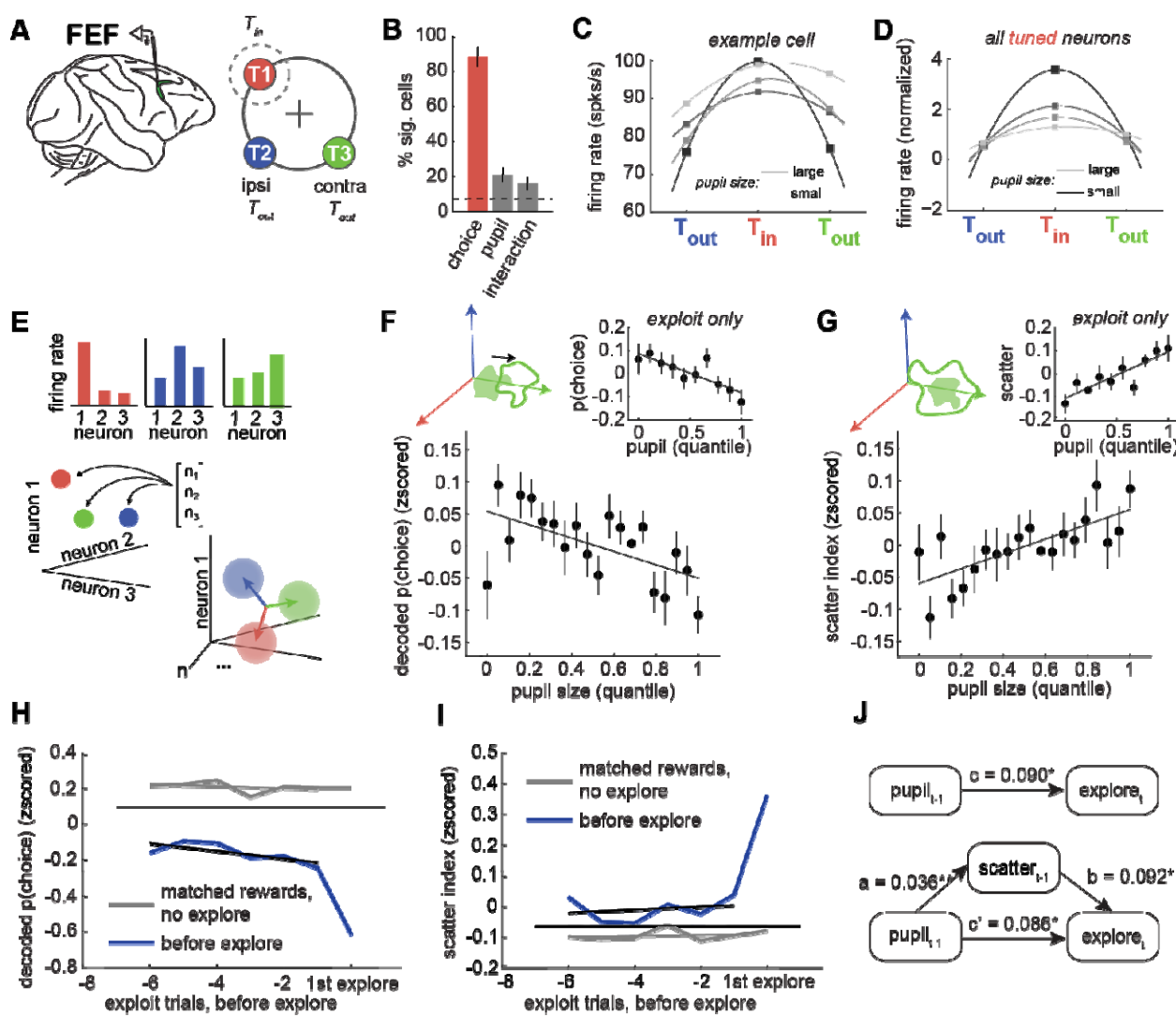
392
393
394 **Figure 3. The onset of exploration is phase-locked to pupil size.** A) Average pupil size over
395 sequences of exploit trials before the onset of exploration (black line) and sequences with
396 matched rewards, but no exploration at the end (gray line). Lines: GLM fit. B) Cartoon illustrating
397 how oscillations in arousal (top) could interact with reward history (middle), to regulate
398 exploration. The bottom panel illustrates a hypothetical pupil trace that has an additive effect of
399 reward omissions and by oscillating arousal. Exploration (diamond shapes) begins when pupil
400 size reaches a threshold (dotted line). Note that identical patterns of reward delivery and
401 omission have different outcomes, depending on how they align with the phase of arousal (gray
402 = no exploration, blue = exploration). C) Difference in pupil size between the traces in A. D)
403 Phase distribution of pupil size at the onset of exploration (blue) and bootstrapped null
404 distribution (black). The vectors at the center indicate the mean vector direction and length for
405 the trials before exploration (blue) and the matched reward trials (gray). Shaded areas \pm SEM
406 throughout.
407

408 Pupil size predicts flattened neural tuning in prefrontal cortex during exploration

409 To probe the neural mechanisms linking pupil size to exploration, we examined how pupil size
410 predicts neural activity in the FEF (Bruce and Goldberg, 1985; Moore and Armstrong, 2003;
411 Moore and Fallah, 2001; Schall and Hanes, 1993) (**Figure 4A**). We previously reported that
412 exploration is associated with flattened tuning for choice in FEF neurons (Ebitz et al., 2018).
413 While FEF neurons often predict upcoming choices during exploitation, many show reduced
414 choice selectivity during exploration. Pupil size predicted similar changes in in FEF neurons and

415 did so beyond what could be explained by exploratory states themselves. Out of 155 recorded
 416 single neurons, 88 (57%) were tuned for choice (**Figure 4B**; 57%, one sample proportion test: p
 417 < 0.001). These are referred to as "tuned neurons," regardless of whether they were modulated
 418 by pupil size. Among tuned neurons, 21 (24%) were also modulated by pupil size, and 16 (18%)
 419 showed a significant interaction between choice and pupil size. On average, tuning curves
 420 flattened as pupil size increased in both tuned and untuned neurons (**Figure 4C-D**). Among
 421 untuned neurons, an additional 22% (15/67) were significantly modulated by pupil size ($p <$
 422 0.05), with a median regression coefficient (β) of -0.0011 ± 0.063 . This suggests that pupil-
 423 linked mechanisms affect FEF activity even in neurons that are not directly involved in encoding
 424 choice. This may suggest a more domain-general role for arousal in modulating prefrontal
 425 network dynamics.

426



427

428 **Figure 4. Pupil size predicts choice tuning curves and population disorganization.** A)
429 Recordings were made in the FEF. Right: The cartoon illustrates the relative positions of the
430 receptive field target (T_{in} , red) and the ipsilateral and contralateral targets (T_{out} , blue and green).
431 B) Percent of neurons with significant tuning for choice target, pupil size, and the interaction. C)
432 Tuning curve for an example neuron across target locations, separated by pupil size. Lighter =
433 larger pupil. The dashed line indicates the number of neurons expected to be significant by
434 chance at $p < 0.05$. D) Same for all tuned neurons, which refers to the 88 out of 155 FEF
435 neurons that were significantly tuned for choice, regardless of their modulation by pupil size. E)
436 Cartoon illustrating how neural population measures consider patterns of firing rates across
437 neurons as vectors in neural state space. Targeted dimensionality reduction is used to find the
438 hyperplane where the distribution of neural activity across trials best predicts choice. Vectors
439 here are the coding dimensions that separate the choices. F) The decoded choice probability
440 (projection onto the correct coding dimension) plotted as a function of pupil size quantile. Inset:
441 Same for exploit trials alone. G) The scatter index, a measure of the variance in choice-
442 predictive population activity, plotted as a function of pupil size quantile. Inset: Same for exploit
443 trials. H) Decoded choice probability for trials before the onset of exploration (in blue) and trials
444 with matched rewards (in gray). I) Scatter index for trials before the onset of exploration (in blue)
445 and trials with matched rewards (in gray). Error bars and shaded regions \pm SEM. J) Mediation
446 analysis between pupil size, scatter index, and the onset of exploration. Top: Direct model.
447 Bottom: Indirect, mediated model. Asterisks marked significant paths (* $p < 0.01$ ** $p < 0.001$).

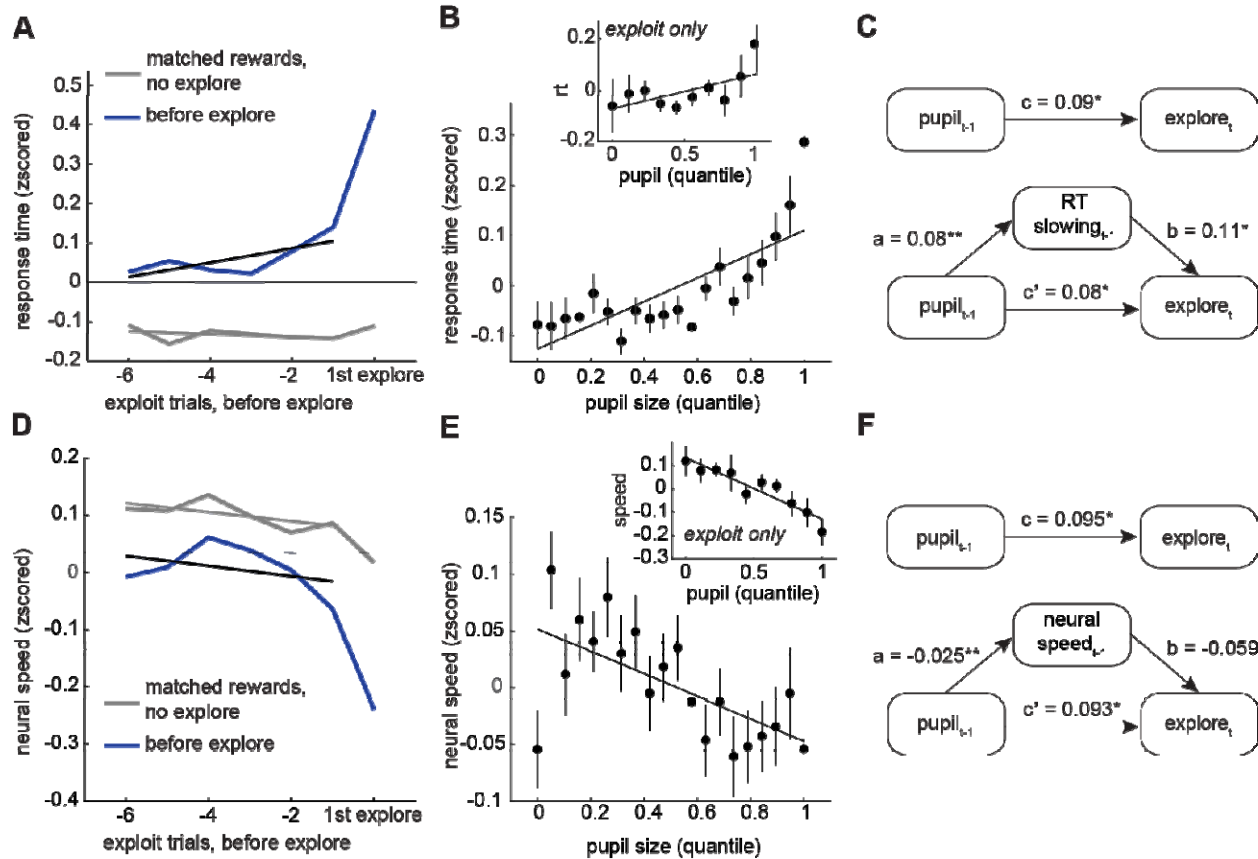
448 Because single neurons are noisy, it is difficult to dissociate the effects of pupil size and
449 exploration at the level of individual cells. However, changes in tuning at the single-neuron level
450 also imply shifts in the organization of the neural population and looking at the population level
451 can allow us to estimate these effects within smaller subsets of the data (Ebitz and Hayden,
452 2021); **Figure 4E**). Indeed, we found that pupil size also predicted changes in how accurately
453 choice information could be decoded from simultaneously recorded populations of FEF neurons.
454 Consistent with our prior results (Ebitz et al., 2018), decoded choice probability was significantly
455 lower during exploration compared to exploitation (paired t-test: both subjects, $p < 0.0001$,
456 **Figure S2A**). Critically, larger pupil size predicted weaker choice encoding both across all trials
457 (**Figure 4F**; GLM: $\beta = -0.032$, $p < 0.0001$). This was not driven by differences between the
458 states because pupil size also predicted choice decoding accuracy within exploit trials alone
459 (GLM: $\beta = -0.037$, $p < 0.005$). There was no significant effect of pupil size on choice
460 decoding within explore trials (GLM: $\beta = -0.003$, $p = 0.77$, **Figure S2B**), which could have been
461 due to differences in trial counts (i.e., explore trials made up only ~15% of total trials) or to floor
462 effects (decoding accuracy was already close to chance in these trials). These findings show
463 that pupil-linked arousal predicts the strength of choice-predictive neural signals in FEF above
464 and beyond what can be explained by differences between the states.

465 In our previous work, we found that decreases in choice-predictive activity were accompanied
466 by increases in variability in FEF population responses to the same choice (Ebitz et al., 2018).

467 We quantified this with the “scatter index”: a measure of the spread within clusters of same-
468 choice population activity (see **Methods**). A high scatter index indicates that neural activity on a
469 given trial was dissimilar to other trials where the same choice was made, whereas a low scatter
470 index indicates that neural activity was tightly clustered. We observed a higher scatter index
471 during exploration compared to exploitation (paired t-test: both subjects, $p < 0.0001$, **Figure**
472 **S2C**). Here, we also found that increasing pupil size predicted an increase in the scatter index in
473 both subject B and subject O (**Figure 4G**; GLM: $\beta = 0.04$, $p < 0.0001$). This effect remained
474 significant and of similar magnitude within exploit trials alone (GLM: $\beta = 0.03$, $p < 0.0005$), again
475 suggesting that the relationship between pupil size and scatter was not an artifact of state
476 differences with pupil size. Pupil size again did not significantly predict the scatter index during
477 explore trials (GLM: $\beta = 0.0006$, $p = 0.94$, **Figure S2D**). Thus, pupil size predicted
478 disorganization of choice-predictive signals in the FEF, at both the level of single neurons and in
479 the population.

480 **Neural disorganization mediates the relationship between pupil size and exploration**

481 To test whether neural population activity, like pupil size, also specifically predicted the onset of
482 exploration, we compared its dynamics in the trials preceding exploration to those in matched-
483 reward control trials. While sudden changes in the decoded choice probability and scatter index
484 were largely aligned with the onset of exploration (as reported previously), these neural
485 measures were at a different average level on the trials preceding exploration, compared to
486 reward-matched controls (**Figure 4H-I**; choice probability, offset = -0.611, $p < 0.001$, $n = 28$;
487 scatter index = 0.258, $p < 0.001$). Reward information did not cause a change in either variable
488 (choice probability, slope = -0.004, $p > 0.5$; scatter index = 0.002, $p > 0.5$), while small, but
489 significant interaction terms suggested that both variables anticipated the onset of exploration
490 (choice probability interaction = -0.058, $p < 0.01$; scatter index interaction: $\beta = 0.040$, $p <$
491 0.001). To determine if these neural measures might explain or mediate some of the
492 relationship between pupil size and exploration, we turned to structural equation modeling
493 (Preacher et al., 2007; Sobel, 1986). We found that the scatter index was a significant mediator
494 of the relationship between pupil size and the onset of exploration (**Figure 4J**; effect of
495 mediation, $ab = 0.003$, $p < 0.005$; full report in Table S1). Together, these results suggest that
496 pupil size predicts disruptions in the organization of prefrontal neural activity that then mediate
497 its relationship with the onset of exploration.



498

499 **Figure 5. Pupil size predicts behavioral and neural slowing.** A) Response time on exploit
500 trials before the onset of exploration (blue) and trials with matched rewards but no exploration
501 (gray). B) Response time plotted as a function of pupil size quantile. Inset: Same for exploit
502 trials alone. C) Mediation analysis between pupil size, response time, and the onset of
503 exploration. Top: Direct model. Asterisks marked significant paths ($*p < 0.01$). Bottom: Indirect,
504 mediated model. D) Neural speed on exploit trials before the onset of exploration (in blue) and
505 trials with matched rewards (in gray). E-F) Same as B-C for neural speed. Shaded areas and
506 error bars \pm SEM.

507

508 Exploration may reflect a critical transition in brain state dynamics

509 Neural systems, like other complex networks, can undergo tipping points—irreversible “critical
510 transitions” between stable operating regimes (O’Byrne and Jerbi, 2022; Scheffer, 2020;
511 Scheffer et al., 2009; Wang et al., 2012). Because exploration occurs as the brain passes from
512 exploiting one target to exploiting another, it is worth considering the possibility that exploration
513 may represent a critical transition in brain states. Indeed, during exploration, we previously
514 reported (Ebitz et al., 2018) several phenomena in the FEF and in behavior that are hallmarks of
515 critical transitions, including a rapid flickering back and forth between choices (Wang et al.,

516 2012), an increase in the variance in neural activity (Scheffer et al., 2009), and a disruption of
517 long-term neuronal autocorrelations that suggests that passing through exploration causes time-
518 irreversible changes in the FEF network (Scheffer, 2020). However, there is another classic
519 feature of critical transitions that we did not consider: an early warning signal known as “critical
520 slowing”. As the system nears the tipping point, the dynamics within the system begin to flatten
521 out in preparation for the change. As a result, the systems’ processes slow down and take
522 longer to trace the same paths (Scheffer et al., 2009). Therefore, we next asked if there was any
523 evidence that decision-making slowed down in advance exploration in this dataset.

524

525 To test for critical slowing, we examined two measures of decision speed: one behavioral and
526 one neural. First, we looked at response time, a measure of how long it takes the brain to
527 generate saccadic decisions. Response time was not only slower in the trials before exploration,
528 compared to matched-reward control trials (**Figure 5A-C**; GLM offset = 0.39, $p < 0.0001$, $n = 28$), but it slowed down over trials before the onset of exploration (interaction = 0.05, $p < 0.001$).
529 Second, we looked at the mean rate of change in neural population choice signals during the
530 decision process (“neural speed”, see **Methods**). Neural speed was only weakly correlated with
531 response time across sessions (mean = -0.07, min = -0.36, max = 0.09, Pearson’s correlation),
532 suggesting that the measures were complementary, rather than redundant. Like response time,
533 neural speed was also significantly slower on average in the trials before exploration, compared
534 to matched-reward controls (**Figure 5D-F**; GLM offset = -0.17, $p < 0.0001$, $n = 28$). However,
535 unlike response time, neural speed did not show a significant slowing trend over trials
536 (interaction = -0.01, $p = 0.08$). Although the notion that the brain may be subject to critical
537 tipping points is controversial (O’Byrne and Jerbi, 2022), these results are consistent with the
538 idea that exploration could reflect a critical transition between exploiting one option and
539 exploiting another.

541

542 We first asked whether slowing effects could be better explained by the typical reward histories
543 that precede exploration, rather than internal states like arousal. However, reward history alone
544 did not have a significant effect on either neural or behavioral slowing (response time: slope of
545 matched-reward trials = 0.0002, $p > 0.5$; neural speed: slope = -0.018, $p > 0.1$). This suggests
546 that some internal variable, like arousal, could be driving increased slowing and, perhaps, also
547 the systems’ proximity to a tipping point. Indeed, increasing pupil size predicted slower
548 response times (**Figure 5B**; GLM beta = 0.08, $p < 0.0001$, $n = 28$ sessions), even within periods
549 of exploitation (beta = 0.05, $p < 0.0001$). The same was true of neural slowing (**Figure 5E**; all

550 trials: beta = -0.03, p < 0.0005; exploit only: beta = -0.09, p < 0.0001). Further, structural
551 equation modeling revealed that both measures of slowing mediated the relationship between
552 pupil size and the onset of exploration (**Figure 5C and F**; Table S2-3). In sum, the pupil-linked
553 mechanisms that anticipated exploration included both a disorganization of neural activity and a
554 slowing of decision-related computations in brain and behavior—hallmarks of a system
555 approaching a critical transition.

556 **Discussion**

557 Random decision-making is a powerful strategy for exploration (Dayan and Daw, 2008; Ebitz et
558 al., 2018; Gershman, 2019; Wilson et al., 2021, 2014) that is linked to disorganized patterns of
559 neural activity in the prefrontal cortex (Ebitz et al., 2018; Muller et al., 2019; Wilson et al., 2021).
560 Here, we sought to identify some of the neurobiological mechanisms that drive random
561 exploration and its neural signatures. We found that pupil size, a peripheral correlate of
562 autonomic arousal, predicted exploration and certain measures of neural population activity
563 previously linked to exploration. Consistent with previous studies (Jepma and Nieuwenhuis,
564 2011a), pupil size was generally larger during exploration, compared to exploitation. However,
565 there was also a complex temporal relationship, where pupil size ramped up between periods of
566 exploration and decreased during exploration. As a result, pupil size was largest at the
567 beginning or “onset” of exploration and explained variance in the onset of exploration that could
568 not be explained by other variables. Together, these results suggest that pupil-linked
569 mechanisms may play a role in driving the brain into an exploratory state.

570

571 Our behavioral results largely replicate previous findings linking exploration to increased pupil
572 size (Jepma and Nieuwenhuis, 2011a). However, where we found gradual ramping before
573 exploration and sudden constriction after, Jepma and Nieuwenhuis (2011) reported an abrupt (if
574 modest) increase of pupil size at the onset of exploration and then a gradual decrease at the
575 return to exploitation. The discrepancy may be due to differences in the operational definition of
576 exploration. Jepma and Nieuwenhuis (2011) fit an RL model to behavior and defined “explore
577 choices” as the choices that were not reward-maximizing according to the model. This definition
578 conflates exploration with errors of reward maximization. A strategy that is non-reward-
579 maximizing would produce choices that are orthogonal to value, not consistently bad. Here, we
580 used an HMM to identify latent explore and exploit states on the basis of the temporal profiles of
581 choices alone, with no assumptions on the underlying value computations. This allowed us to
582 dissociate the effects of reward history from the explore/exploit choice labels. We reported here

583 (Figure 1C), and in previous studies (Chen et al., 2021; Ebitz et al., 2018), that HMM labels
584 outperform RL labels in explaining behavioral and neural measures, suggesting that the HMM
585 may more accurately separate distinct neural and behavioral states. If the HMM allows for more
586 precise identification of exploratory and exploitative choices, it would follow that it also allows for
587 more precise reconstruction of the temporal relationship between the pupil and exploration.

588

589 The precision of our explore/exploit labels revealed that the U-shaped relationship between
590 pupil size and exploration was caused by a refractory constriction in the pupil. When exploration
591 was plotted as a function of pupil size, the relationship appeared non-linear: both small- and
592 large-pupil choices were more likely to be exploratory. This superficially resonated with the idea
593 of a U-shaped relationship between arousal and task performance (i.e. the “Yerkes-Dodson
594 curve”; (Aston-Jones and Cohen, 2005; Yerkes and Dodson, 1908): perhaps reliable exploitation
595 is only possible at intermediate levels of arousal. However, when we examined the temporal
596 relationship between exploration and pupil size, we found that pupil size only predicted the
597 onset of exploration, the first explore choice in a sequence. Small-pupil explore choices
598 happened because starting to explore seemed to “reset” the level of pupil-linked arousal,
599 causing it to quickly fall below baseline. If increased pupil size promotes a transition to
600 exploration, then it is possible that post-exploration constriction represents a refractory period
601 for exploration. Given that uncertainty grows with time in this task (and in all dynamic
602 environments), it may not be smart to start to explore again immediately after you have just
603 explored. A refractory period could ensure that non-reward-maximizing explore choices are
604 deployed only when needed. Future work is needed to test this hypothesis and to determine the
605 cognitive and/or neurobiological mechanisms at play.

606

607 Before exploration, we observed an oscillatory dynamic that was about twice as fast as the 10
608 trials it took the pupil to recover after exploration. This 0.06-0.09 Hz oscillation entrained the
609 onset of exploration: onsets tended to occur during the rising phase of pupil size, whereas
610 identical trial sequences that did not result in exploration were on the opposite phase. This
611 implies that it is the confluence of pupil size, pupil phase, and trial history that best predicts the
612 onset of exploration. This result reinforces the idea that arousal or arousal-linked mechanisms
613 help trigger random exploration (Ebitz and Moore, 2019; Gilzenrat et al., 2010; Reimer et al.,
614 2016), rather than just tracking the reward-linked variables that make exploration more
615 probable. It is also notable that the period of the pupil oscillation was close to the frequency of
616 the Mayer wave: an oscillation in blood pressure that entrains other autonomic measures,

617 including respiration and heart rate (Borjon et al., 2016a; Japundzic et al., 1990; Julien, 2020,
618 2006; Kamiya et al., 2005). There is precedent for the idea that behavior can be entrained by
619 the Mayer wave: in marmosets, fluctuations in arousal predict the spontaneous onset of a call
620 (Borjon et al., 2016a). This paper argued that the Mayer wave may function to organize vocal
621 communication by bringing the system closer to the threshold for transitioning from inaction to
622 action. It is possible that oscillations in the pupil and pupil-linked mechanisms function the same
623 way here, organizing important state changes in time. In parallel, pupil-linked mechanisms seem
624 to anticipate other state transitions, including belief updating (Filipowicz et al., 2020; O'Reilly et
625 al., 2013), task disengagement (Kane et al., 2017), and other behavioral state changes (Bouret
626 and Sara, 2005). Together, these results suggest an important role for pupil-linked mechanisms
627 in driving successful transitions between certain neural and behavioral states.

628

629 Critically, pupil size and pupil oscillations did not predict all state transitions here, but only the
630 transition into exploration. What kinds of state transitions might be entrained by pupil-linked
631 arousal? It is possible that the pupil may have a special relationship with certain “critical” kinds
632 of transitions. Critical transitions are abrupt, large-scale, and irreversible changes in the
633 dynamics and behavior of complex systems, like the brain. As these systems go from being in
634 one conformation (i.e. always choosing the left option) into another conformation (i.e. always
635 choosing the right), the system dynamics that support the old state have to disappear and the
636 new dynamics have to emerge. During this brief transitory period, when both dynamics co-exist
637 in the system, certain signatures can be observed in the system. We previously reported that
638 the exploration was accompanied by abrupt changes in neural population activity, certain
639 patterns of noise in brain and behavior, and disruptions in long-term neuronal autocorrelations:
640 all observations that could be interpreted as suggesting that exploration is a critical transition in
641 the brain (Ebitz et al., 2018). Here, we found that pupil size predicts these features of neural
642 activity and also an prominent “early warning sign” of critical transitions: a slowing, in brain and
643 behavior, of the decision process. While there are certain patterns of activity in FEF that predict
644 response speed (Hauser et al., 2018; Yao and Vanduffel, 2023), here we identified *independent*
645 neural and behavioral measures of decision speed that both mediated the relationship between
646 pupil size and exploration. Notably, pupil size also predicted slower neural and behavioral
647 responses within exploit-only trials, suggesting that these effects are not an artifact of
648 differences between explore and exploit states. This suggests that these effects may reflect a
649 domain-general influence of arousal on cognitive dynamics, consistent with the idea that
650 fluctuations in pupil-linked neuromodulation shape the temporal structure of decision-making in

651 general, beyond any role in state transitions. In this view, the transition into exploration in FEF
652 may reflect an extremum of these domain-general arousal effects—a tipping point—rather than
653 signals that are highly specific to state transitions. Together these results suggest that pupil-
654 linked arousal pushes neural and behavioral states to a critical tipping point and highlights the
655 crucial role of pupil-linked mechanisms in changing the dynamics of the brain.

656

657 What underlying, pupil-linked mechanisms could support critical transitions? Changes in pupil
658 diameter coincide with neuromodulator system activity, especially norepinephrine (NE) and
659 acetylcholine (Breton-Provencher and Sur, 2019; de Gee et al., 2020; Joshi et al., 2016; Joshi
660 and Gold, 2020; Murphy et al., 2014; Reimer et al., 2016). At the neuronal level, central NE
661 flattens tuning curves, at least in the auditory cortex (Martins and Froemke, 2015), though it may
662 have different effects in non-cortical structures (Manella et al., 2017). Here, we made a parallel
663 observation: as pupil size increases, neuronal tuning curves_flattened and choice-predictive
664 neural population activity became disorganized. These results resonate with a particularly
665 influential theory of NE function: the idea that NE release may facilitate “resets” in cortical
666 networks in order to effect long-lasting changes in brain and behavior (Aston-Jones and Cohen,
667 2005; Bouret and Sara, 2005). More recent studies seem to consistently report that elevated
668 levels of NE predict an increase in behavioral variability, while pharmacological blockade of NE
669 receptors reduces variability (Chen et al., 2023; Kane et al., 2017; Sadacca et al., 2017; Tervo
670 et al., 2014). In combination with the present study, these results could suggest that phasic NE
671 signaling functions to push the brain towards a critical tipping point where it is better able to
672 transition from one regime to another. In this view, behavioral variability would be linked to NE
673 not because NE increases variability directly, but because the brain is more likely to transition
674 into a high variability regime after it is released. Of course, pupil size is also associated with
675 other neuromodulatory systems, cognitive factors, and other measures of arousal. Thus, future
676 work is needed to identify the neurobiological mechanisms that underpin the relationship
677 between pupil size and critical transitions that we report here.

678 Materials and Methods

679 *Surgical and electrophysiological procedures.* All procedures were approved by the Stanford
680 University Institutional Animal Care and Use Committee. Subjects were two male rhesus
681 macaques, surgically-prepared with head restraint prostheses, craniotomies, and recording
682 chambers under isoflurane anesthesia via techniques described previously (Ebitz et al., 2018).

683 Following surgery, analgesics were used to minimize discomfort, and antibiotics were delivered
684 prophylactically. After recovery, subjects were acclimated to the laboratory and head restraint,
685 then placed on controlled access to fluids and trained to perform the task.

686 In order to train the animals on the explore/exploit task a gradual procedure was used in which
687 the two animals were first trained to make saccadic eye movements in exchange for liquid
688 rewards. Once the animals reliably made controlled eye movements to a single target (generally
689 within 1–2 days), a second target was introduced, and the animals were free to choose between
690 them. At the outset, each target was associated with a probability of reward (initially 10% and
691 90%), which was reversed in blocks at the experimenter's discretion. Over a period of 2–4
692 months, the difference in reward probabilities between the targets was gradually reduced, the
693 blocks transitioned into gradual reward probability shifts (reward walks), and a third target was
694 introduced. The speed and order of these changes depended on each animal's performance
695 and engagement with the task. One animal (monkey O) was naïve to laboratory tasks prior to
696 this experiment, whereas the second (monkey B) had been previously trained on covert and
697 overt attention tasks, but not on any prior value-based tasks.

698 Recording sites were located within the FEF, which was identified via a combination of
699 anatomical and functional criteria. The location of recording sites in the anterior bank of the
700 arcuate sulcus was verified histologically in one subject and via microstimulation in both
701 subjects (Ebitz et al., 2018). Recordings were conducted with 16-channel U-probes (Plexon),
702 located such that each contact was within gray matter at an FEF site. An average of 20 units
703 were recorded in each session (131 single units, 443 multi units; 576 total units across 28
704 sessions).

705 *General behavioral procedures.* Eye position and pupil size were monitored at 1000 Hz via an
706 infrared eye tracking system (SR Research; Eyelink). The manufacturer's standard methods for
707 calculating pupil area were used. MATLAB (Psychtoolbox-3; (Kleiner et al., 2007)) was used to
708 display stimuli and record behavioral responses and pupil size measurements. Task stimuli
709 were presented against a dark gray background (7 cd/m²) on a 47.5 cm wide LCD monitor
710 (Samsung; 120 Hz refresh rate, 1680 x 1050 resolution), located 34 cm in front of the subject.

711 *Three-armed bandit task.* The subjects performed a sequential decision-making task in which
712 they chose between 3 targets whose values changed over time. The subject first fixated a
713 central fixation square (0.5° stimulus, +/- 1.5-2° of error) for a variable interval (450-750ms). At

714 any point within 2s after the onset of the targets, subjects indicated their choice by making a
715 saccade to one of the targets and fixating it (+/- 3°) for 150 ms. Reward magnitude was fixed
716 within session (0.2-0.4 μ L). Reward probability was determined by the current reward probability
717 of the chosen target, which changed independently over trials for each of the three targets. On
718 every correct trial, each target had a 10% chance of the reward parameter changing either up or
719 down by a fixed step of 0.1, bounded at 0.1 and 0.9. Because rewards were variable,
720 independent, and probabilistic, the subjects could only infer the values of the different targets by
721 sampling them and integrating noisy experienced rewards over multiple trials.

722 *General analysis procedures.* Data were analyzed with custom software in MATLAB. Unless
723 otherwise noted, all t-tests were paired, two-sided t-tests, and generalized linear models were
724 run on raw data, with session number coded as a dummy variable to account for session-to-
725 session variability. Model comparison was based on standard methods that involve calculating
726 the likelihood of the data and Akaike information criteria (AIC) of each model, then using AIC
727 weights to identify (1) the model that is most likely to minimize information loss, and (2) the
728 relative likelihood of competing models to do the same (Burnham and Anderson, 2004). For
729 analyses of any behavioral or neural variables on the trials before or after exploration,
730 continuous runs of exploit trials were required. The values of behavioral and neural variables
731 were z-scored within a session to facilitate comparisons across sessions. In the results section,
732 we refer to a z-score of 0 as “baseline”. The 200 ms window immediately preceding target onset
733 was chosen as the analysis epoch for all choice-predictive neural measures. A longer, whole-
734 trial epoch was chosen for neural speed analyses (0 to 500 ms) following target presentation.
735 Firing rates were computed per trial.

736 *Pupil size.* Pupil size was measured during the first 200 ms of fixation, a time at which the eye
737 was fixed at a known point on the screen, illumination was identical across trials, and
738 anticipatory changes in the pupil were minimal. To remove any blinks or movement artifacts,
739 trials where pupil size or the change in pupil size from the first time bin of this epoch to the last
740 was +/- 6 standard deviations from average were eliminated from further analyses. A total of
741 178 trials (out of 21,793, approximately 0.8% of observations) were outliers.

742 *Hidden Markov Model.* To identify when subjects were exploring versus exploiting, we employed
743 a hidden Markov model (Chen et al., 2021; Ebitz et al., 2018). In this framework, choices Y_t are
744 treated as emissions from a latent decision-making state z_t , which can either be an explore or
745 one of the multiple exploit states.

746 The emission model for exploration assumed a uniform probability of selecting any option:

$$p(y_t = k | z_t = \text{explore}) = \frac{1}{N_k}$$

747

748 Where N_k is the total number of options. In contrast, exploit states deterministically emitted
749 choices to the exploited option i :

$$p(y_t = k | z_t = \text{exploit}_i, k = i) = 1$$

$$p(y_t = k | z_t = \text{exploit}_i, k \neq i) = 0$$

750
751 Latent state transitions followed a Markov process, such that the probability of the current state
752 depended only on the previous state:

$$p(z_t | z_{t-1}, y_{t-1}, \dots, z_1, y_1) = p(z_t | z_{t-1})$$

753

754 To reduce model complexity, parameters were shared across exploit states, and subjects were
755 assumed to begin in the explore state. The final HMM included only two free parameters: the
756 probability of persisting in exploration and the probability of persisting in exploitation. The model
757 was fit using expectation-maximization with 20 random restarts, and the solution maximizing the
758 observed data log-likelihood was selected. The most probable sequence of latent states was
759 recovered using the Viterbi algorithm.

760 *Reinforcement learning model.* To compare goal state labels derived from an RL and HMM
761 model, we employed a Rescorla-Wagner model. This was fit using maximum likelihood
762 estimation. The value of each option is iteratively updated according to:

$$V_{i,t+1} = V_{i,t} + \alpha(r_t - V_{i,t})$$

763

764 Where $V_{i,t}$ is the value of option i at time t , r_t is the reward at time t , and α represents the fitted
765 learning rate, which determines how much the difference between the predicted and actual

766 reward (the prediction error) influences value. To make a decision, the values are passed
767 through a softmax decision rule:

$$p_{i,t} = \frac{\exp(\beta V_{i,t})}{\sum_{j=1:n} \exp(\beta V_{j,t})}$$

768
769 Where n is the total number of available options, and β is the inverse temperature, which
770 controls the level of random noise in decision-making. After (Daw et al., 2006; Jepma and
771 Nieuwenhuis, 2011a; Pearson et al., 2009), decisions that were not reward maximizing were
772 labeled as exploratory (i.e. any decision where $V_{chosen,t}$ was not the maximum V at time t).

773 *Generalized Linear Model (GLM)*. To examine the relationship between behavioral and neural
774 variables, we employed generalized linear models (GLMs). These models were fit using
775 maximum likelihood estimation. Each dependent variable (i.e., scatter index, response time,
776 or choice probability) was modeled as a linear combination of predictors:

$$Y_i = \beta_0 + \beta_1 \cdot explore\ state_i + \beta_2 \cdot pupil\ size_i + \beta_3 \cdot (explore\ state_i \times pupil\ size_i) + \varepsilon_i$$

777
778 Where Y_i is the dependent variable on trial i , β_0 is the intercept, and $\beta_1, \beta_2, \beta_3$ are regression
779 coefficients quantifying the influence of the corresponding predictors (e.g., explore state, pupil
780 size, and their interactions). ε_i is the residual error term.

781 In analyses where categorical variables (e.g., explore state: 0 = exploit, 1 = explore) were used
782 as predictors, these were coded as binary dummy variables. Models were fit using the identity
783 link function and assumed normally distributed errors.

784 *Learning Index*. To investigate whether learning differed with pupil size within the exploratory
785 choices, we calculated a learning index that captured the effect of rewards experienced during
786 exploration on future choices. Because reward effects decay exponentially quickly (Lau and
787 Glimcher, 2008), a 1-trial-ahead index should capture most of the variability in how much is
788 learned between trial types. The equation was:

$$\text{learning index}_t = \frac{p(\text{switch}_{t+1} \mid \text{reward}_t) - p(\text{switch}_{t+1} \mid \text{no reward}_t)}{p(\text{switch}_{t+1})}$$

789

790 *Lagged change in pupil size.* To determine whether exploration impacted pupil size, we
791 measured the change in pupil size (Δ pupil) between pairs of trials that either were or were not
792 separated by at least 1 explore trial. Segments of twenty-five consecutive trials were identified
793 that either included a single bout of exploration or did not include exploration. For each pair of
794 trials within these sequences, we then measured the change in pupil size between the first
795 exploit trial of the sequence (t1) and the remaining exploit trials in the sequence (t2:25). This
796 was repeated for all unique pairs of trials that met our selection criteria.

797

798 *Matched reward trials.* To test whether the rising trend in pupil size before exploration is best
799 explained by reward history, we identified trial sequences with identical reward and state
800 histories that did not end in exploration (“matched rewards”). For each onset of exploration
801 preceded by at least 6 exploit trials, we searched for identical sequences of exploit trials, with
802 identical reward histories, that did not end in exploration. We chose 6 previous trials because
803 this was the longest sequence of reward history we could regularly match within the majority of
804 sessions (we could find at least 10 matched sequences in 96% [27/28] of sessions for 6 trials
805 sequences; that dropped to 75% [21/28] at 7 trials). Identical results were obtained with other
806 sequence lengths, though these analyses included fewer sessions.

807

808 *Mediation analysis.* To determine if the predictive relationship between pupil size and
809 exploration was mediated by other variables, we used structural equation modeling to test for
810 mediation. Mediation analyses involve fitting three regression models. The first model measures
811 the total effect (c) of the independent variable (here, pupil size) on the independent variable
812 (here, onset of exploration):

$$\text{Explore}_t = \gamma_1 + c(\text{Pupil}_{t-1}) + \epsilon_1$$

813

814 In these equations, γ represents the intercept for each equation, while ϵ represents the error of
815 the model. Note that the estimated parameter c will include both direct effects of pupil size on
816 exploration, but also indirect effects that may be mediated by other variables. Therefore, we

817 also fit a second model that tests if the independent variable also predicts a potential mediator
818 variable (here, neural network scatter):

$$\text{Scatter}_{t-1} = \gamma_2 + a(\text{Pupil}_{t-1}) + \epsilon_2$$

819
820 Model parameter a thus captures the effect of pupil size on the mediator. Finally, a third model
821 estimates the unique contributions of both the potential mediator (scatter, b) and the
822 independent variable (pupil size, c'), now controlling for the mediator:

$$\text{Explore}_t = \gamma_3 + b(\text{Scatter}_{t-1}) + c'(\text{Pupil}_{t-1}) + \epsilon_3$$

823
824 A drop between c and c' indicates that the effect of the independent variable (pupil) on the
825 dependent variable (exploration) is reduced when the mediating variable is considered. The
826 mediation effect (the indirect effect of the pupil size on the onset of exploration via the mediating
827 factor) can also be estimated directly, via taking the product of the coefficients a and b. Sobel's
828 test is used to determine the significance of the mediation path (Sobel, 1986).

829
830 *Phase analysis.* To determine if the onset of exploration happened at a specific phase of pupil
831 size over trials, we performed a wavelet analysis. Because this method only assumes local
832 stationarity, it is more suitable than other methods for analyzing pupil size, which tended to
833 ramp over trials. A wavelet was constructed by multiplying a complex sine wave (frequency = 5
834 trials) with a Gaussian envelope ($\mu = 0$, $\sigma = \text{cycles} / (2\pi \times \text{frequency})$, cycles = 5; (Cohen, 2014)).
835 The wavelet was convolved with the baseline pupil size time series and the phase of the signal
836 was calculated on each trial (Matlab; angle). Standard circular statistics were used to measure
837 the differences between phase distributions for explore onsets and reward-matched controls
838 (Zar, 1999) and the phase alignment within these trial types (Berens, 2009). The latter was also
839 verified via comparison with bootstrapped null distributions (1000 samples).

840 *Targeted dimensionality reduction.* Neural state spaces have as many dimensions as there are
841 recorded neurons, but converging evidence suggests (1) that the neural states that are
842 observed in practice are generally confined to a lower-dimensional “manifold”, and (2) that task-
843 relevant information is encoded by a small number of dimensions in that manifold. Because we
844 wanted to isolate the effects of arousal on choice-related activity from well-known effects of
845 arousal on neural activity (Ebitz and Platt, 2015; McGinley et al., 2015; Pfeffer et al., 2022;
846 Podvalny et al., 2021; Reimer et al., 2016, 2014; van Kempen et al., 2019; Waschke et al.,

847 2019), we focused all our neural population analyses on activity within the choice-predictive
848 subspace, rather than on neural activity more broadly.

849
850 To do this, we used targeted dimensionality reduction to identify the choice-predictive
851 dimensions of the neural state space (Cohen and Maunsell, 2010; Cunningham and Yu, 2014;
852 Ebitz et al., 2018; Peixoto et al., 2021). Specifically, we used multinomial logistic regression
853 (Matlab; mnrrfit, mnrvval, (Hastie et al., 2009)) to identify the separating hyperplanes that best
854 discriminated each choice from the alternative choices. This is equivalent to fitting a system of
855 binary classifiers of the form:

$$p(\text{choice} = k \mid X) = \frac{1}{1 - \exp^{-\beta_k X}}$$

856
857 Where one classifier discriminates target 1 choices from targets 2 and 3 and a second
858 discriminates target 2 choices from targets 1 and 3. The classifier that discriminates target 3
859 from targets 1 and 2 is then just the negative of target 1 and target 2. These axes span the
860 subspace in which neural activity best predicts choice. Classifiers were trained on firing rates
861 from an epoch that began when the targets appeared and ended at the time of the saccade.
862 Mean imputation was used for the small number of occasions where a unit was not held for the
863 whole duration of the session (~3% of trials, ~12% of units) and a small fraction of units were
864 omitted from these analyses because their mean firing rates were less than 2 spikes/s, which
865 makes their weights difficult to identify (~8% of units).

866
867 *Choice Probability Decoding.* Within the choice-predictive subspace, the distance from the
868 separating hyperplanes (the vectors illustrated in **Figure 4E**) are the decoding vectors: the
869 vectors along which we can project neural activity in order to decode the log odds of choice.
870 This projection is equivalent to the decoded choice probability from the multinomial logistic
871 regression model and this is the figure we took as the decoded choice probability in **Figures 3F**
872 and **3H**. We evaluated decoding accuracy by measuring how often the most-likely choice
873 predicted by the model coincided with the choice the subject made.

874 *Scatter index.* The scatter index measures how much choice-predictive population neural
875 activity is clustered between trials with the same choice (Ebitz et al., 2018). It is calculated by
876 measuring the average Euclidean distance of each trial from all other trials where the same

877 choice was made and dividing it by the average Euclidean distance to all other trials where a
878 different choice was made:

$$\text{scatter} = \frac{d_{\text{within}}}{d_{\text{between}}}$$

879
880 Each trial thus has its own scatter index value, with a value of 1 indicating no difference in
881 clustering between same-choice and different-choice trials, and a value less than 1 indicating
882 greater clustering with same-choice trials compared to different-choice trials.

883 *Neural speed.* To determine how the speed of the decision-making process changed before and
884 during exploration, we calculated the rate of change in neural states within the choice-predictive
885 subspace during the first 400 ms following target presentation. Each trial's neural activity was
886 sampled in non-overlapping 20 ms bins and then projected into the choice-predictive subspace.
887 The change in neural activity within the subspace was then calculated between each pair of
888 samples. Finally, the changes were averaged together across the trial and normalized to the bin
889 width to produce an average rate of change in choice-predictive activity for that trial.

890 **Acknowledgments**

891 This work was supported by the Natural Sciences and Engineering Research Council of Canada
892 (Discovery Grant RGPIN-2020-05577), the Fonds de Recherche du Québec–Santé (Junior 1
893 Chercheur-Boursier 284309 to R.B.E.), the Jacobs Foundation (Research Fellowship, seed
894 grant to R.B.E.), and CIFAR Azrieli Global Scholars (seed grant to R.B.E.), the National Eye
895 Institute (R01-EY014924 to T.M.), and l'Institut de valorisation des données (fellowship to K.J.).

References

Aston-Jones G, Cohen JD. 2005. AN INTEGRATIVE THEORY OF LOCUS COERULEUS-NOREPINEPHRINE FUNCTION: Adaptive Gain and Optimal Performance. *Annu Rev Neurosci* **28**:403–450. doi:10.1146/annurev.neuro.28.061604.135709

Berens P. 2009. CircStat: A MATLAB Toolbox for Circular Statistics. *J Stat Softw* **31**:1–21. doi:10.18637/jss.v031.i10

Bijleveld E, Custers R, Aarts H. 2009. The Unconscious Eye Opener: Pupil Dilation Reveals Strategic Recruitment of Resources Upon Presentation of Subliminal Reward Cues. *Psychol Sci* **20**:1313–1315. doi:10.1111/j.1467-9280.2009.02443.x

Borjon JI, Takahashi DY, Cervantes DC, Ghazanfar AA. 2016a. Arousal dynamics drive vocal production in marmoset monkeys. *J Neurophysiol* **116**:753–764. doi:10.1152/jn.00136.2016

Borjon JI, Takahashi DY, Cervantes DC, Ghazanfar AA. 2016b. Arousal dynamics drive vocal production in marmoset monkeys. *J Neurophysiol* **116**:753–764. doi:10.1152/jn.00136.2016

Bouret S, Sara SJ. 2005. Network reset: a simplified overarching theory of locus coeruleus noradrenaline function. *Trends Neurosci* **28**:574–582. doi:10.1016/j.tins.2005.09.002

Bradley MM, Miccoli L, Escrig MA, Lang PJ. 2008. The pupil as a measure of emotional arousal and autonomic activation. *Psychophysiology* **45**:602–607. doi:10.1111/j.1469-8986.2008.00654.x

Breton-Provencher V, Sur M. 2019. Active control of arousal by a locus coeruleus GABAergic circuit. *Nat Neurosci* **22**:218–228. doi:10.1038/s41593-018-0305-z

Bruce CJ, Goldberg ME. 1985. Primate frontal eye fields. I. Single neurons discharging before saccades. *J Neurophysiol* **53**:603–635. doi:10.1152/jn.1985.53.3.603

Burnham KP, Anderson DR, editors. 2004. Model Selection and Multimodel Inference. New York, NY: Springer. doi:10.1007/b97636

Chen CS, Knep E, Han A, Ebitz RB, Grissom NM. 2021. Sex differences in learning from exploration. *eLife* **10**:e69748. doi:10.7554/eLife.69748

Chen CS, Mueller D, Knep E, Ebitz RB, Grissom NM. 2023. Dopamine and norepinephrine differentially mediate the exploration-exploitation tradeoff. doi:10.1101/2023.01.09.523322

Clewett D, Gasser C, Davachi L. 2020. Pupil-linked arousal signals track the temporal organization of events in memory. *Nat Commun* **11**:4007. doi:10.1038/s41467-020-17851-9

Cohen MR, Maunsell JHR. 2010. A Neuronal Population Measure of Attention Predicts Behavioral Performance on Individual Trials. *J Neurosci* **30**:15241–15253. doi:10.1523/JNEUROSCI.2171-10.2010

Cohen MX. 2014. Analyzing neural time series data: theory and practice. MIT press.

Costa VD, Averbeck BB. 2020. Primate Orbitofrontal Cortex Codes Information Relevant for Managing Explore–Exploit Tradeoffs. *J Neurosci* **40**:2553–2561. doi:10.1523/JNEUROSCI.2355-19.2020

Costa VD, Rudebeck PH. 2016. More than Meets the Eye: the Relationship between Pupil Size and Locus Coeruleus Activity. *Neuron* **89**:8–10. doi:10.1016/j.neuron.2015.12.031

Cunningham JP, Yu BM. 2014. Dimensionality reduction for large-scale neural recordings. *Nat Neurosci* **17**:1500–1509. doi:10.1038/nn.3776

Daw ND, O'Doherty JP, Dayan P, Seymour B, Dolan RJ. 2006. Cortical substrates for exploratory decisions in humans. *Nature* **441**:876–879. doi:10.1038/nature04766

Dayan P, Daw ND. 2008. Decision theory, reinforcement learning, and the brain. *Cogn Affect*

Behav Neurosci **8**:429–453. doi:10.3758/CABN.8.4.429

de Gee JW, Tsetsos K, Schwabe L, Urai AE, McCormick D, McGinley MJ, Donner TH. 2020. Pupil-linked phasic arousal predicts a reduction of choice bias across species and decision domains. *eLife* **9**:e54014. doi:10.7554/eLife.54014

Ding L, Hikosaka O. 2006. Comparison of Reward Modulation in the Frontal Eye Field and Caudate of the Macaque. *J Neurosci* **26**:6695–6703. doi:10.1523/JNEUROSCI.0836-06.2006

Ebitz RB, Albaran E, Moore T. 2018. Exploration Disrupts Choice-predictive Signals and Alters Dynamics in Prefrontal Cortex. *Neuron* **97**:450-461.e9. doi:10.1016/j.neuron.2017.12.007

Ebitz RB, Hayden BY. 2021. The population doctrine in cognitive neuroscience. *Neuron* **109**:3055–3068. doi:10.1016/j.neuron.2021.07.011

Ebitz RB, Moore T. 2019. Both a Gauge and a Filter: Cognitive Modulations of Pupil Size. *Front Neurosci* **9**.

Ebitz RB, Pearson JM, Platt ML. 2014. Pupil size and social vigilance in rhesus macaques. *Front Neurosci* **8**.

Ebitz RB, Platt ML. 2015. Neuronal Activity in Primate Dorsal Anterior Cingulate Cortex Signals Task Conflict and Predicts Adjustments in Pupil-Linked Arousal. *Neuron* **85**:628–640. doi:10.1016/j.neuron.2014.12.053

Ebitz RB, Sleezer BJ, Jedema HP, Bradberry CW, Hayden BY. 2019. Tonic exploration governs both flexibility and lapses. *PLOS Comput Biol* **15**:e1007475. doi:10.1371/journal.pcbi.1007475

Ebitz RB, Tu JC, Hayden BY. 2020. Rules warp feature encoding in decision-making circuits. *PLOS Biol* **18**:e3000951. doi:10.1371/journal.pbio.3000951

Eldar E, Cohen JD, Niv Y. 2013. The effects of neural gain on attention and learning. *Nat Neurosci* **16**:1146–1153. doi:10.1038/nn.3428

Fiete IR, Fee MS, Seung HS. 2007. Model of Birdsong Learning Based on Gradient Estimation by Dynamic Perturbation of Neural Conductances. *J Neurophysiol* **98**:2038–2057. doi:10.1152/jn.01311.2006

Filipowicz AL, Glaze CM, Kable JW, Gold JI. 2020. Pupil diameter encodes the idiosyncratic, cognitive complexity of belief updating. *eLife* **9**:e57872. doi:10.7554/eLife.57872

Gershman SJ. 2019. Uncertainty and Exploration. *Decis Wash DC* **6**:277–286. doi:10.1037/dec0000101

Gilzenrat MS, Nieuwenhuis S, Jepma M, Cohen JD. 2010. Pupil diameter tracks changes in control state predicted by the adaptive gain theory of locus coeruleus function. *Cogn Affect Behav Neurosci* **10**:252–269. doi:10.3758/CABN.10.2.252

Graves JE, Egré P, Pressnitzer D, de Gardelle V. 2021. An implicit representation of stimulus ambiguity in pupil size. *Proc Natl Acad Sci* **118**:e2107997118. doi:10.1073/pnas.2107997118

Hastie T, Tibshirani R, Friedman J. 2009. The Elements of Statistical Learning, Springer Series in Statistics. New York, NY: Springer. doi:10.1007/978-0-387-84858-7

Hauser CK, Zhu D, Stanford TR, Salinas E. 2018. Motor selection dynamics in FEF explain the reaction time variance of saccades to single targets. *eLife* **7**:e33456. doi:10.7554/eLife.33456

Japundzic N, Grichois M-L, Zitoun P, Laude D, Elghozi J-L. 1990. Spectral analysis of blood pressure and heart rate in conscious rats: effects of autonomic blockers. *J Auton Nerv Syst* **30**:91–100. doi:10.1016/0165-1838(90)90132-3

Jepma M, Nieuwenhuis S. 2011a. Pupil Diameter Predicts Changes in the Exploration–Exploitation Trade-off: Evidence for the Adaptive Gain Theory. *J Cogn Neurosci* **23**:1587–1596. doi:10.1162/jocn.2010.21548

Jepma M, Nieuwenhuis S. 2011b. Pupil diameter predicts changes in the exploration-exploitation trade-off: Evidence for the adaptive gain theory. *J Cogn Neurosci* **23**:1587–1596.

Joshi S, Gold JI. 2020. Pupil Size as a Window on Neural Substrates of Cognition. *Trends Cogn Sci* **24**:466–480. doi:10.1016/j.tics.2020.03.005

Joshi S, Li Y, Kalwani R, Gold JI. 2016. Relationships between pupil diameter and neuronal activity in the locus coeruleus, colliculi, and cingulate cortex. *Neuron* **89**:221–234. doi:10.1016/j.neuron.2015.11.028

Julien C. 2020. An update on the enigma of Mayer waves. *Cardiovasc Res* **116**:e210–e211. doi:10.1093/cvr/cvz327

Julien C. 2006. The enigma of Mayer waves: Facts and models. *Cardiovasc Res* **70**:12–21. doi:10.1016/j.cardiores.2005.11.008

Jurewicz K, Sleezer BJ, Mehta PS, Hayden BY, Ebitz RB. 2022. Irrational choices via a curvilinear representational geometry for value. doi:10.1101/2022.03.31.486635

Kamiya A, Hayano J, Kawada T, Michikami D, Yamamoto K, Ariumi H, Shimizu S, Uemura K, Miyamoto T, Aiba T, Sunagawa K, Sugimachi M. 2005. Low-frequency oscillation of sympathetic nerve activity decreases during development of tilt-induced syncope preceding sympathetic withdrawal and bradycardia. *Am J Physiol-Heart Circ Physiol* **289**:H1758–H1769. doi:10.1152/ajpheart.01027.2004

Kane GA, Vazey EM, Wilson RC, Shenhav A, Daw ND, Aston-Jones G, Cohen JD. 2017. Increased locus coeruleus tonic activity causes disengagement from a patch-foraging task. *Cogn Affect Behav Neurosci* **17**:1073–1083. doi:10.3758/s13415-017-0531-y

Kaske EA, Chen CS, Meyer C, Yang F, Ebitz B, Grissom N, Kapoor A, Darrow DP, Herman AB. 2022. Prolonged physiological stress is associated with a lower rate of exploratory learning that is compounded by depression. *Biol Psychiatry Cogn Neurosci Neuroimaging*. doi:10.1016/j.bpsc.2022.12.004

Kleiner M, Brainard DH, Pelli D. 2007. What's new in Psychtoolbox-3? *Perception* **36**:1–16.

Koss MC. 1986. Pupillary dilation as an index of central nervous system α 2-adrenoceptor activation. *J Pharmacol Methods* **15**:1–19. doi:10.1016/0160-5402(86)90002-1

Lau B, Glimcher PW. 2008. Value Representations in the Primate Striatum during Matching Behavior. *Neuron* **58**:451–463. doi:10.1016/j.neuron.2008.02.021

Laurie V-J, Shourkeshti A, Chen CS, Herman A, Grissom N, Ebitz RB. 2025. Persistent Decision-Making in Mice, Monkeys, and Humans. *bioRxiv* 2024.05.07.592970. doi:10.1101/2024.05.07.592970

Loewenfeld IE. 1999. The Pupil: Anatomy, Physiology, and Clinical Applications. Butterworth-Heinemann.

Manella LC, Petersen N, Linster C. 2017. Stimulation of the Locus Ceruleus Modulates Signal-to-Noise Ratio in the Olfactory Bulb. *J Neurosci* **37**:11605–11615. doi:10.1523/JNEUROSCI.2026-17.2017

Martins ARO, Froemke RC. 2015. Coordinated forms of noradrenergic plasticity in the locus coeruleus and primary auditory cortex. *Nat Neurosci* **18**:1483–1492. doi:10.1038/nn.4090

McGinley MJ, David SV, McCormick DA. 2015. Cortical Membrane Potential Signature of Optimal States for Sensory Signal Detection. *Neuron* **87**:179–192. doi:10.1016/j.neuron.2015.05.038

Moore T, Armstrong KM. 2003. Selective gating of visual signals by microstimulation of frontal cortex. *Nature* **421**:370–373. doi:10.1038/nature01341

Moore T, Fallah M. 2001. Control of eye movements and spatial attention. *Proc Natl Acad Sci U S A* **98**:1273–1276. doi:10.1073/pnas.98.3.1273

Muller TH, Mars RB, Behrens TE, O'Reilly JX. 2019. Control of entropy in neural models of

environmental state. *eLife* **8**:e39404. doi:10.7554/eLife.39404

Murphy PR, Vandekerckhove J, Nieuwenhuis S. 2014. Pupil-Linked Arousal Determines Variability in Perceptual Decision Making. *PLOS Comput Biol* **10**:e1003854. doi:10.1371/journal.pcbi.1003854

Nassar MR, Rumsey KM, Wilson RC, Parikh K, Heasly B, Gold JI. 2012. Rational regulation of learning dynamics by pupil-linked arousal systems. *Nat Neurosci* **15**:1040–1046. doi:10.1038/nn.3130

O'Byrne J, Jerbi K. 2022. How critical is brain criticality? *Trends Neurosci*. doi:10.1016/j.tins.2022.08.007

O'Reilly JX, Schüffelgen U, Cuell SF, Behrens TEJ, Mars RB, Rushworth MFS. 2013. Dissociable effects of surprise and model update in parietal and anterior cingulate cortex. *Proc Natl Acad Sci* **110**:E3660–E3669. doi:10.1073/pnas.1305373110

Pearson JM, Hayden BY, Raghavachari S, Platt ML. 2009. Neurons in posterior cingulate cortex signal exploratory decisions in a dynamic multi-option choice task. *Curr Biol CB* **19**:1532–1537. doi:10.1016/j.cub.2009.07.048

Peixoto D, Verhein JR, Kiani R, Kao JC, Nuyujukian P, Chandrasekaran C, Brown J, Fong S, Ryu SI, Shenoy KV, Newsome WT. 2021. Decoding and perturbing decision states in real time. *Nature* **591**:604–609. doi:10.1038/s41586-020-03181-9

Pfeffer T, Keitel C, Kluger DS, Keitel A, Russmann A, Thut G, Donner TH, Gross J. 2022. Coupling of pupil- and neuronal population dynamics reveals diverse influences of arousal on cortical processing. *eLife* **11**:e71890. doi:10.7554/eLife.71890

Pisupati S, Chartarifsky-Lynn L, Khanal A, Churchland AK. 2021. Lapses in perceptual decisions reflect exploration. *eLife* **10**:e55490. doi:10.7554/eLife.55490

Platt ML, Glimcher PW. 1999. Neural correlates of decision variables in parietal cortex. *Nature* **400**:233–238. doi:10.1038/22268

Podvalny E, King LE, He BJ. 2021. Spectral signature and behavioral consequence of spontaneous shifts of pupil-linked arousal in human. *eLife* **10**:e68265. doi:10.7554/eLife.68265

Preacher KJ, Rucker DD, Hayes AF. 2007. Addressing Moderated Mediation Hypotheses: Theory, Methods, and Prescriptions. *Multivar Behav Res* **42**:185–227. doi:10.1080/00273170701341316

Preuschoff K, 't Hart B, Einhäuser W. 2011. Pupil Dilation Signals Surprise: Evidence for Noradrenaline's Role in Decision Making. *Front Neurosci* **5**.

Reimer J, Froudarakis E, Cadwell CR, Yatsenko D, Denfield GH, Tolias AS. 2014. Pupil Fluctuations Track Fast Switching of Cortical States during Quiet Wakefulness. *Neuron* **84**:355–362. doi:10.1016/j.neuron.2014.09.033

Reimer J, McGinley MJ, Liu Y, Rodenkirch C, Wang Q, McCormick DA, Tolias AS. 2016. Pupil fluctuations track rapid changes in adrenergic and cholinergic activity in cortex. *Nat Commun* **7**:13289. doi:10.1038/ncomms13289

Roesch MR, Olson CR. 2007. Neuronal Activity Related to Anticipated Reward in Frontal Cortex. *Ann N Y Acad Sci* **1121**:431–446. doi:10.1196/annals.1401.004

Sadacca B, Wikenheiser AM, Schoenbaum G. 2017. Towards a theoretical role for tonic norepinephrine in the orbitofrontal cortex in facilitating flexible learning. *Neuroscience* **345**:124–129. doi:10.1016/j.neuroscience.2016.04.017

Schall JD, Hanes DP. 1993. Neural basis of saccade target selection in frontal eye field during visual search. *Nature* **366**:467–469. doi:10.1038/366467a0

Scheffer M. 2020. Critical Transitions in Nature and Society, Princeton Studies in Complexity. Princeton University Press.

Scheffer M, Bascompte J, Brock WA, Brovkin V, Carpenter SR, Dakos V, Held H, van Nes EH, Rietkerk M, Sugihara G. 2009. Early-warning signals for critical transitions. *Nature*

461:53–59. doi:10.1038/nature08227

Schultz W, Preuschoff K, Camerer C, Hsu M, Fiorillo CD, Tobler PN, Bossaerts P. 2008. Explicit neural signals reflecting reward uncertainty. *Philos Trans R Soc B Biol Sci* **363**:3801–3811. doi:10.1098/rstb.2008.0152

Slooten JCV, Jahfari S, Knapen T, Theeuwes J. 2018. How pupil responses track value-based decision-making during and after reinforcement learning. *PLOS Comput Biol* **14**:e1006632. doi:10.1371/journal.pcbi.1006632

Sobel ME. 1986. Some New Results on Indirect Effects and Their Standard Errors in Covariance Structure Models. *Sociol Methodol* **16**:159–186. doi:10.2307/270922

Tervo DGR, Proskurin M, Manakov M, Kabra M, Vollmer A, Branson K, Karpova AY. 2014. Behavioral Variability through Stochastic Choice and Its Gating by Anterior Cingulate Cortex. *Cell* **159**:21–32. doi:10.1016/j.cell.2014.08.037

Urai AE, Braun A, Donner TH. 2017. Pupil-linked arousal is driven by decision uncertainty and alters serial choice bias. *Nat Commun* **8**:14637. doi:10.1038/ncomms14637

van Kempen J, Loughnane GM, Newman DP, Kelly SP, Thiele A, O'Connell RG, Bellgrove MA. 2019. Behavioural and neural signatures of perceptual decision-making are modulated by pupil-linked arousal. *eLife* **8**:e42541. doi:10.7554/eLife.42541

Wang R, Dearing JA, Langdon PG, Zhang E, Yang X, Dakos V, Scheffer M. 2012. Flickering gives early warning signals of a critical transition to a eutrophic lake state. *Nature* **492**:419–422. doi:10.1038/nature11655

Waschke L, Tune S, Obleser J. 2019. Local cortical desynchronization and pupil-linked arousal differentially shape brain states for optimal sensory performance. *eLife* **8**:e51501. doi:10.7554/eLife.51501

Wilson RC, Bonawitz E, Costa VD, Ebitz RB. 2021. Balancing exploration and exploitation with information and randomization. *Curr Opin Behav Sci, Computational cognitive neuroscience* **38**:49–56. doi:10.1016/j.cobeha.2020.10.001

Wilson RC, Geana A, White JM, Ludvig EA, Cohen JD. 2014. Humans use directed and random exploration to solve the explore-exploit dilemma. *J Exp Psychol Gen* **143**:2074–2081. doi:10.1037/a0038199

Wu HG, Miyamoto YR, Castro LNG, Ölveczky BP, Smith MA. 2014. Temporal structure of motor variability is dynamically regulated and predicts motor learning ability. *Nat Neurosci* **17**:312–321. doi:10.1038/nn.3616

Yao T, Vanduffel W. 2023. Spike rates of frontal eye field neurons predict reaction times in a spatial attention task. *Cell Rep* **42**:112384. doi:10.1016/j.celrep.2023.112384

Yerkes RM, Dodson JD. 1908. The relation of strength of stimulus to rapidity of habit-formation. *J Comp Neurol Psychol* **18**:459–482. doi:10.1002/cne.920180503

Yokoi A, Weiler J. 2022. Pupil diameter tracked during motor adaptation in humans. *J Neurophysiol* **128**:1224–1243. doi:10.1152/jn.00021.2022

Zar JH. 1999. Biostatistical analysis. Pearson Education India.

896 **Table S1**

897 Regression coefficients and p values for the mediation analysis testing whether the scatter
898 index mediates the relationship between pupil size and the onset of exploration. Related to
899 **Figure 4J.**

		pupil _{t-1} → scatter _{t-1} → explore _t	
		est. coefficient	p value <
Total effect	c	0.090	0.005
Effect on mediator	a	0.036	0.0005
Unique mediator effect	b	0.092	0.005
Indirect effect	ab	0.003 (z = 2.70*)	0.005
Direct effect	c'	0.086	0.005

900 *Sobel's test

901

902 **Table S2**

903 Regression coefficients and p values for the mediation analysis testing whether response time
904 slowing mediates the relationship between pupil size and the onset of exploration on the next
905 trial. Related to **Figure 5C.**

		pupil _{t-1} → RT slowing _{t-1} → explore _t	
		est. coefficient	p value <
Total effect	c	0.090	0.005
Effect on mediator	a	0.078	0.0001
Unique mediator effect	b	0.106	0.0005
Indirect effect	ab	0.008 (z = 3.48*)	0.0005
Direct effect	c'	0.080	0.01

906 *Sobel's test

907 **Table S3**

908 Regression coefficients and p values for the mediation analysis testing whether neural slowing
909 mediates the relationship between pupil size and the onset of exploration on the next trial.
910 Related to **Figure 5F**.

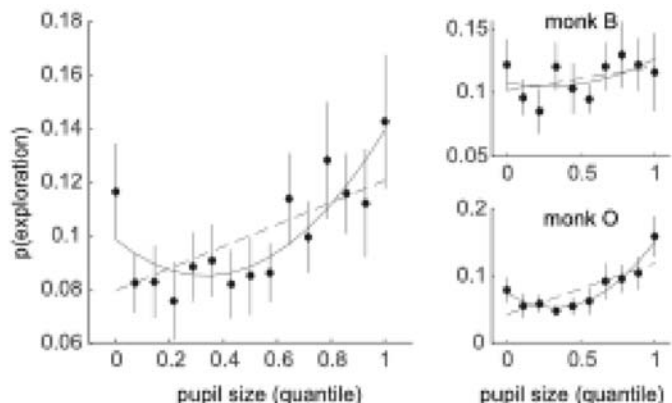
pupil _{t-1} → neural slowing _{t-1} → explore _t			
		est. coefficient	p value <
Total effect	c	0.095	0.005
Effect on mediator	a	-0.025	0.0005
Unique mediator effect	b	-0.059	0.06
Indirect effect	ab	0.001 (z = 1.69*)	0.05
Direct effect	c'	0.093	0.005

911 *Sobel's test

912

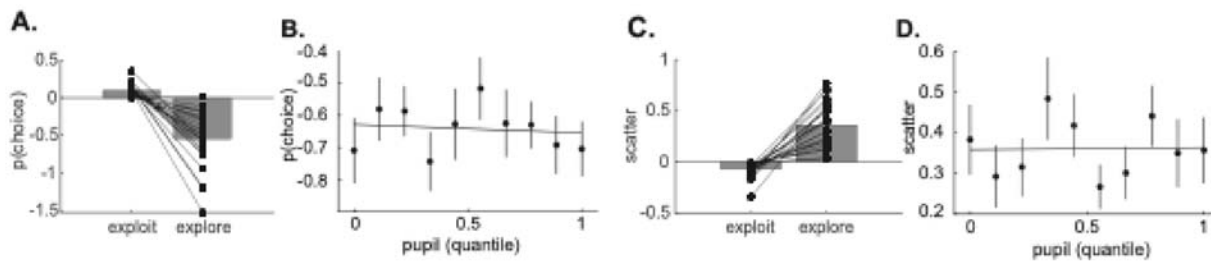
913

914 **Figure S1**
915



916
917 **Figure S1.** Same as **Figure 1E**, but without first explore trials.

918 **Figure S2**



919
920 **Figure S2.** Decoded choice probability and scatter index across behavioral states and pupil
921 size. (A) Decoded choice probability (projection onto the correct coding dimension) for exploit
922 and explore states. Dots represent individual sessions, with lines connecting values from the
923 same session across states. (B) Decoded choice probability plotted as a function of pupil size
924 quantile for explore trials alone. (C) Scatter index, a measure of variance in choice-predictive
925 population activity, for exploit and explore states, with lines connecting values from the same
926 session across states. (D) The scatter index plotted as a function of pupil size quantile for
927 explore trials.
928